Mechanism of soft X-ray continuum radiation from low-energy pinch discharges of hydrogen and ultra-low field ignition of solid fuels

R. Mills[1], J. Lotoski[1], Y. Lu[1]

[1]Brilliant Light Power, Inc., 493 Old Trenton Road, Cranbury, NJ 08512, USA

Abstract

EUV continuum radiation (10–30 nm) arising only from very low energy pulsed pinch gas discharges comprising some hydrogen was first observed at BlackLight Power, Inc. (BLP) and reproduced at the Harvard Center for Astrophysics (CfA). The source was determined to be due to the transition of H to the lower-energy hydrogen or hydrino state H(1/4) whose emission matches that observed wherein alternative sources were eliminated. The identity of the catalyst that accepts $3 \cdot 27.2$ eV from the H to cause the H to H(1/4) transition was determined to HOH versus 3H. The mechanism was elucidated using different oxide-coated electrodes that were selective in forming HOH versus plasma forming metal atoms as well as from the intensity profile that was a mismatch for the multi-body reaction required during 3H catalysis. The HOH catalyst was further shown to give EUV radiation of the same nature by igniting a solid fuel comprising a source of H and HOH catalyst by passing a low voltage, high current through the fuel to produce explosive plasma. No chemical reaction can release such high-energy light. No high field existed to form highly ionized ions that could give radiation in this EUV region that persisted even without power input. This plasma source serves as strong evidence for the existence of the transition of H to hydrino H(1/4) by HOH as the catalyst and a corresponding new power source wherein initial extraordinarily brilliant light-emitting prototypes are already producing photovoltaic generated electrical power. The hydrino product of a catalyst reaction of atomic hydrogen was analyzed by multiple spectroscopic techniques. Moreover, m H catalyst was identified to be active in astronomical sources such as the Sun, stars, and interstellar medium wherein the characteristics of hydrino match those of the dark matter of the universe.

Keywords: hydrogen EUV continua, dark matter

1 Introduction

Atomic hydrogen is predicted to form fractional Rydberg energy states $\mathrm{H}(1/p)$ called "hydrino atoms" wherein $n=\frac{1}{2},\frac{1}{3},\frac{1}{4},...,\frac{1}{p}$ ($p \le 137$ is an integer) replaces the well-known parameter $n=$ integer in the Rydberg equation for hydrogen excited states. The transition of H to a stable hydrino state $\mathrm{H}\left[\frac{a_{\mathrm{H}}}{p=m+1}\right]$ having a binding energy of $p^2 \cdot 13.6$ eV occurs by a nonradiative resonance energy transfer of $m \cdot 27.2$ eV (m is an integer) to a matched energy acceptor. By the same mechanism, the nascent H_2O molecule (not hydrogen bonded in solid, liquid, or gaseous state) may serve as a catalyst by accepting 81.6 eV (m=3) to form an intermediate that decays with the emission of a continuum band with a short wavelength cutoff of 10.1 nm and energy of 122.4 eV [1]. The continuum radiation band at 10.1 nm and going to longer wavelengths for theoretically predicted transitions of H to lower-energy, so called "hydrino" state H(1/4), was observed only arising from pulsed pinch gas discharges comprising some hydrogen first at BlackLight Power, Inc. (BLP) and reproduced at the Harvard Center for Astrophysics (CfA) by P. Cheimets and P. Daigneau [2–6].

Under a study contracted by GEN3 Partners, spectra of high current pinch discharges in pure hydrogen and helium were recorded in the EUV region at the Harvard Smithsonian Center for Astrophysics (CfA) in an attempt to reproduce experimental results published by BlackLight Power, Inc. (BLP) showing predicted continuum radiation due to hydrogen in the 10–30 nm region. Alternative explanations were considered to the claimed interpretation of the continuum radiation as being that emitted during transitions of H to lower-energy states (hydrinos). Continuum radiation was observed at CfA in the 10–30 nm region that matched BLP's results. Considering the low energy of 5.2 J per pulse, the observed radiation in the energy range of about 120 eV to 40 eV, reference experiments and analysis of plasma gases, cryofiltration to remove contaminants, and spectra of the electrode metal, no conventional explanation was found to be plausible including contaminants, thermal electrode metal emission regarding electron temperature, and Bremsstrahlung, ion recombination, molecular or molecular ion band radiation, and instrument artifacts involving radicals and energetic ions reacting at the CCD and H_2 re-radiation at the detector chamber. Moreover, predicted selective extraordinarily high-kinetic energy H was observed by the corresponding Doppler broadening of the Balmer α line [5].

In this paper, we report the results of the elucidation of the nature of the catalyst of the H to H(1/4) transition being HOH versus 3H using electrodes that have hydrogen reducible versus irreducible oxide coats as well as explosive plasma formed by high current detonation of a solid fuel source of H and HOH catalyst, absent high electric fields that can form highly ionized ions. The hydrino reaction is a powerful new energy source. We show that the reaction rate to form

hydrinos becomes massive with the application of a low voltage, high current to H_2O-based solid fuels causing them to violently explode in a brilliant flash of white light. The spectrum is that of the Sun at about 50,000 times the intensity. Initial prototypes to generate extraordinary optical power by the formation of hydrino (shown herein to be dark matter) are already producing photovoltaic generated electrical power. By further performing EUV spectroscopy on energetic material NH_4NO_3 we show that the mechanism of the shock wave produced by the detonation is high energy and having power released from the formation of hydrinos as supported by previously reported calorimetry and analytical studies [7]. Furthermore, we demonstrate the occurrence of *m*H catalyst reactions to form hydrinos in the laboratory as evidenced by the observation of EUV radiation from a solid fuel comprising a highly conductive material and a source of hydrogen from hydrocarbon wax. Then, we further analyze astrophysical evidence to support atomic *m*H as a pervasive catalyst in bodies comprised of atomic H.

2 Classical theory

Classical physical laws predict that atomic hydrogen may undergo a catalytic reaction with certain species, including itself, that can accept energy in integer multiples of the potential energy of atomic hydrogen, $m \cdot 27.2$ eV, wherein m is an integer. The predicted reaction involves a resonant, nonradiative energy transfer from otherwise stable atomic hydrogen to the catalyst capable of accepting the energy. The product is H(1/p), fractional Rydberg states of atomic hydrogen called "hydrino atoms," wherein n=1/2, 1/3, 1/4,…, 1/p ($p \leq 137$ is an integer) replaces the well-known parameter n=integer in the Rydberg equation for hydrogen excited states. Each hydrino state also comprises an electron, a proton, and a photon, but the field contribution from the photon increases the binding energy rather than decreasing it corresponding to energy desorption rather than absorption. Since the potential energy of atomic hydrogen is 27.2 eV, *m*H atoms serve as a catalyst of $m \cdot 27.2$ eV for another $(m+1)$th H atom [1]. For example, a H atom can act as a catalyst for another H by accepting 27.2 eV from it via through-space energy transfer such as by magnetic or induced electric dipole-dipole coupling to form an intermediate that decays with the emission of continuum bands with short wavelength cutoffs and energies of $m^2 \cdot 13.6 \text{ eV}\left(\frac{91.2}{m^2} \text{ nm}\right)$. In addition to atomic H, a molecule that accepts $m \cdot 27.2$ eV from atomic H with a decrease in the magnitude of the potential energy of the molecule by the same energy may also serve as a catalyst. The potential energy of H_2O is 81.6 eV [1]. Then, by the same mechanism, the nascent H_2O molecule (not hydrogen bonded in solid, liquid, or gaseous state) formed by a thermodynamically favorable reduction of a metal oxide is predicted to serve

as a catalyst to form $\mathrm{H}(1/4)$ with an energy release of 204 eV, comprising an 81.6 eV transfer to HOH and a release of continuum radiation with a cutoff at 10.1 nm (122.4 eV).

In the H-atom catalyst reaction involving a transition to the $\mathrm{H}\left[\frac{a_{\mathrm{H}}}{p=m+1}\right]$ state, mH atoms serve as a catalyst of $m\cdot 27.2$ eV for another $(m+1)$th H atom. Then, the reaction between $m+1$ hydrogen atoms whereby m atoms resonantly and nonradiatively accept $m\cdot 27.2$ eV from the $(m+1)$th hydrogen atom such that mH serves as the catalyst is given by

$$m\cdot 27.2\text{ eV}+mH+H\rightarrow mH^{+}_{fast}+me^{-}+H*\left[\frac{a_H}{m+1}\right]+m\cdot 27.2\text{ eV} \quad (1)$$

$$H*\left[\frac{a_H}{m+1}\right]\rightarrow H\left[\frac{a_H}{m+1}\right]+[(m+1)^2-1^2]\cdot 13.6\text{ eV}-m\cdot 27.2\text{ eV} \quad (2)$$

$$mH^{+}_{fast}+me^{-}\rightarrow mH+m\cdot 27.2\text{ eV} \quad (3)$$

And, the overall reaction is

$$H\rightarrow H\left[\frac{a_H}{p=m+1}\right]+[(m+1)^2-1^2]\cdot 13.6\text{ eV} \quad (4)$$

The catalysis reaction $(m=3)$ regarding the potential energy of nascent H_2O [1] is

$$81.6\text{ eV}+\mathrm{H_2O}+H[a_H]\rightarrow 2H^{+}_{fast}+\mathrm{O^{-}}+\mathrm{e^{-}}+H*\left[\frac{a_H}{4}\right]+81.6\text{ eV} \quad (5)$$

$$H*\left[\frac{a_H}{4}\right]\rightarrow H\left[\frac{a_H}{4}\right]+122.4\text{ eV} \quad (6)$$

$$2H^{+}_{fast}+\mathrm{O^{-}}+\mathrm{e^{-}}\rightarrow \mathrm{H_2O}+81.6\text{ eV} \quad (7)$$

And, the overall reaction is

$$H[a_H]\rightarrow H\left[\frac{a_H}{4}\right]+81.6\text{ eV}+122.4\text{ eV} \quad (8)$$

After the energy transfer to the catalyst (equations (1) and (5)), an intermediate $\mathrm{H}*\left[\frac{a_{\mathrm{H}}}{m+1}\right]$ is formed having the radius of the H atom and a central field of m+1 times the central field of a proton. The radius is predicted to decrease as the electron undergoes radial acceleration to a stable state having a radius of 1/(m+1) the radius of the uncatalyzed hydrogen atom, with the release of $m^2\cdot 13.6\,\mathrm{eV}$ of energy. The extreme-ultraviolet continuum radiation band due to the $\mathrm{H}*\left[\frac{a_{\mathrm{H}}}{m+1}\right]$ intermediate (e.g. equation (2) and equation (6)) is predicted to have a short wavelength cutoff and energy $E_{\left(H\rightarrow H\left[\frac{a_H}{p=m+1}\right]\right)}$ given by

$$E_{\left(H\rightarrow H\left[\frac{a_H}{p=m+1}\right]\right)} = m^2 \cdot 13.6 \text{ eV}; \quad \lambda_{\left(H\rightarrow H\left[\frac{a_H}{p=m+1}\right]\right)} = \frac{91.2}{m^2} \text{ nm} \tag{9}$$

and extending to longer wavelengths than the corresponding cutoff. Here the extreme-ultraviolet continuum radiation band due to the decay of the H*[a_H/4] intermediate is predicted to have a short wavelength cutoff at $E=m^2 \cdot 13.6 = 9 \cdot 13.6 = 122.4$ eV (10.1 nm) [where $p=m+1=4$ and $m=3$ in equation (9)] and extending to longer wavelengths. The continuum radiation band at 10.1 nm and going to longer wavelengths for the theoretically predicted transition of H to lower-energy, so called "hydrino" state H(1/4), was observed only arising from pulsed pinch gas discharges comprising some hydrogen [2–6]. Another observation predicted by equations (1) and (5) is the formation of fast, excited state H atoms from recombination of fast H^+. The fast atoms give rise to broadened Balmer α emission. Greater than 50 eV Balmer α line broadening that reveals a population of extraordinarily high-kinetic-energy hydrogen atoms in certain mixed hydrogen plasmas is a well-established phenomenon; however, the mechanism has been controversial in that the conventional view that it is due to field acceleration is not supported by the data and critical tests [8–27]. Rather it is shown that the cause is due to the energy released in the formation of hydrinos [8–27]. Fast H was previously observed in continuum-emitting hydrogen pinch plasmas [5].

Two possible catalysts, *m*H and HOH, could be the source of the band observed in the 10 to 30 nm region. Both species were present. Hydrogen as an added plasma gas was confirmed by the Balmer visible spectral lines, and oxygen from the electrodes was identifiable by characteristic oxygen ion lines [5] wherein the oxygen reacted with H to form HOH at the electrode surface. To test whether HOH is the dominant catalyst, the spectra were recorded of pulsed pinch hydrogen discharges maintained with metal electrodes that each formed an oxide coat that is thermodynamically unreactive to H reduction. These results were compared with the prior results of the observation of the continuum band only arising from pulsed pinch hydrogen-containing discharges with electrodes each having a metal oxide coat that is thermodynamically favorable to undergo H reduction to form HOH catalyst.

Continuum radiation in the 10 to 30 nm region that matched predicted transitions of H to hydrino state H(1/4), was observed only arising from pulsed pinch hydrogen-containing discharges with metal oxides that are thermodynamically favorable to undergo H reduction to form HOH catalyst; whereas, those that are unfavorable did not show any continuum even though the low-melting point metals tested are very favorable to forming metal ion plasmas with strong short-wavelength continua in more powerful plasma sources. Of the two possible catalysts, *m*H and HOH, the latter is more likely based on the behavior with oxide-coated electrodes and the expectation that the intensities of the transitions of H to H(1/(m +1)) show a

profile of H(1/2) with $\lambda \geq 91.2$ nm >H to H(1/3) with $\lambda \geq 22.8$ nm >H to H(1/4) with $\lambda \geq 10.1$ nm due to the lower cross section for n-body collisions with n being 2, 3, and 4, respectively. The HOH catalyst was further shown to give EUV radiation of the same nature by igniting a solid fuel source of H and HOH catalyst by passing a low voltage, high current through the fuel to produce explosive plasma.

It was shown previously that the kinetics of catalysis of H to H(1/4) by HOH catalyst was explosive when a high current such as 10,000–25,000 A was flowed through a solid fuel [28] comprising a source of H and HOH embedded in a highly conductive matrix. The resulting brilliant light-emitting expanding plasma was predicted to emit EUV continuum radiation according to equation (9) when it was expanded into a vacuum chamber such that its atmospheric pressure was dissipated sufficiently to overcome the optical thickness. Such a light source at once overcame any alternative mechanism of the EUV continuum emission such as being due to a high electric field creating highly-charged ions since the voltage of the ignition current source had an applied AC peak voltage of under 15 V. Moreover, chemical reactions are not capable of more than a few eVs; whereas, the continuum radiation was over 70 eV (estimated over 100 eV with shorter wavelengths cutoff by an Al filter). Due to the optical thickness of elements in the plasma, ion emission lines were observed as expected on a continuum radiation background due to continuum absorption and reemission as spectral lines. The same mechanism applies to H pinch plasma emission. In addition to HOH, as predicted, *m*H atoms acting as a catalyst was evidenced by the observation of EUV radiation from a solid fuel comprising a highly conductive material and a source of hydrogen such as a hydrocarbon through which a low voltage, high current was flowed.

Moreover, *m*H catalyst having the most probable transition of H to H(1/2) was shown active in astrophysical sources. Specifically, multi-body collision reactions of H with another serve as a catalyst to form H(1/p) in stars, the Sun, and interstellar medium, all having large amounts of atomic H. Favorable conditions for H-H collisions are a very dense population of atomic H such as in the Sun and stars. The discovery of high-energy continuum radiation from hydrogen as it forms a more stable form has astrophysical implications such as hydrino being a candidate for the identity of dark matter and the corresponding emission being the source of high-energy celestial and stellar continuum radiation [2]. For example, white-dwarf EUV continuum spectra match the profile of the hydrogen pinch plasma.

3 Experimental method

3.1 EUV pinch plasma spectra

The light source and the experimental set up for recording the EUV spectra of low-pressure pulsed plasmas using molybdenum (Mo), tantalum (Ta), tungsten (W), aluminum (Al), and magnesium (Mg) electrodes are shown in figures 1 and 2. The spectra were recorded using a McPherson grazing incidence EUV spectrometer (Model 248/310G) equipped with a platinum-coated 600 g/mm or a platinum-coated 1200 g/mm grating. The angle of incidence was 87°. The wavelength resolution was about 0.05 nm with an entrance slit width of <1 μm. The EUV light was detected by a CCD detector (Andor iDus) cooled to -60 °C. In addition, CfA provided a McPherson 248/310G spectrometer with a platinum-coated 1200 g/mm grating. Both spectrometers and CfA and BLP gratings were used as part of the measurement program [5, 6].

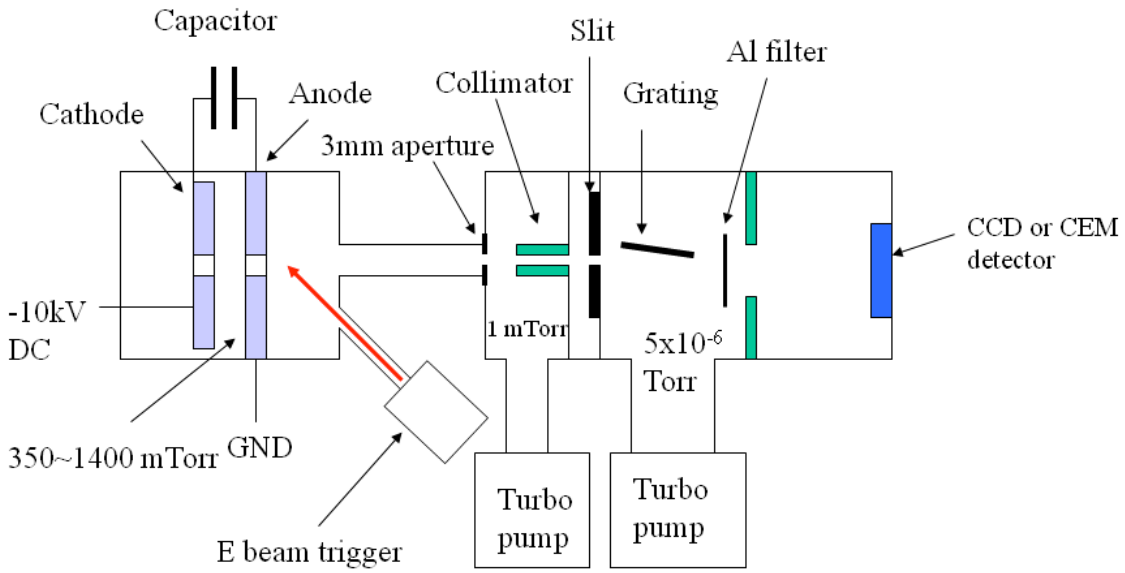

Figure 1. Experimental setup for the high voltage pulsed discharge cell. The source emits its light spectra through an entrance aperture passing through a slit, with the spectra dispersed off a grazing-incidence grating onto a CCD detection system.

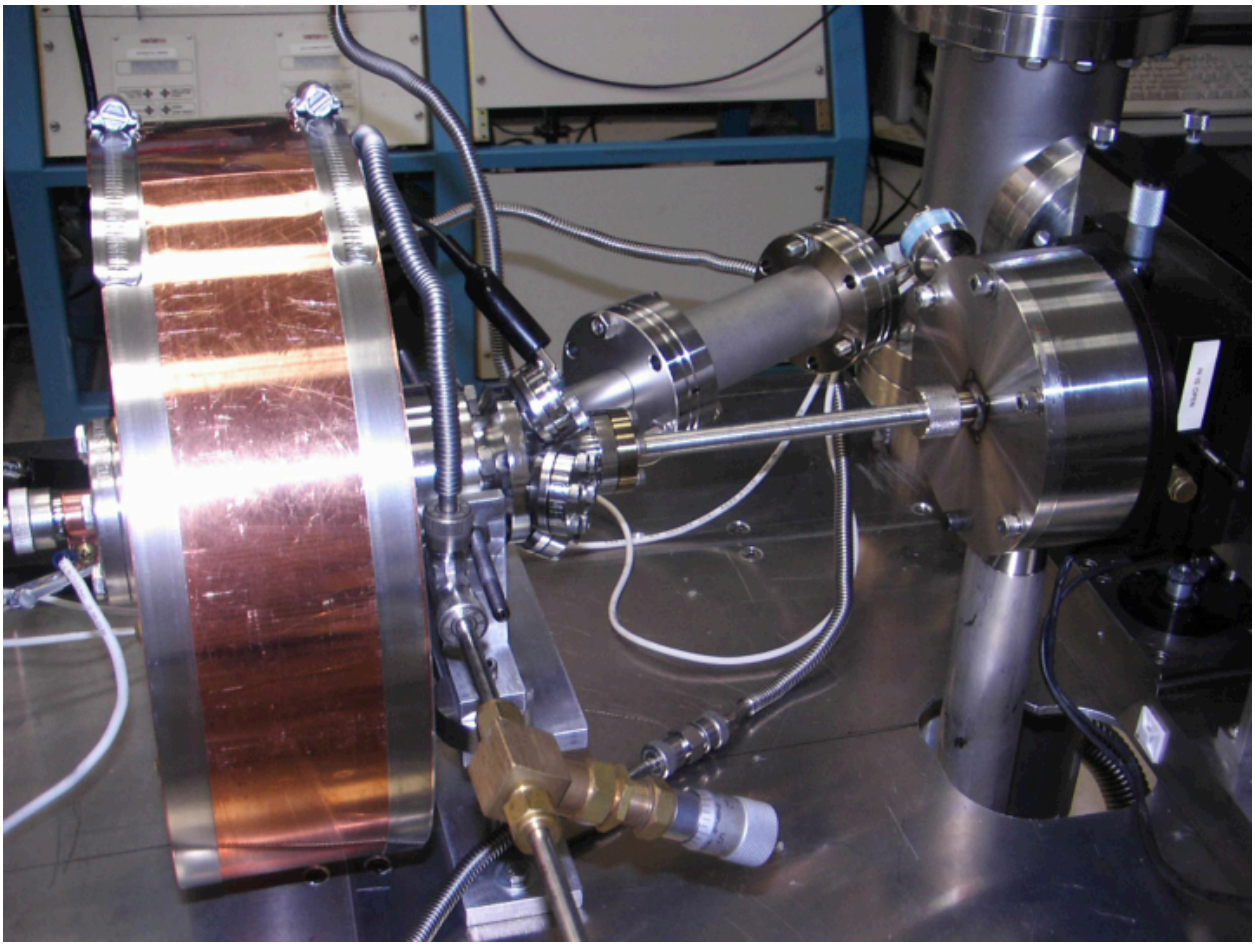

Figure 2. Photograph of the high voltage pulsed discharge light source.

The discharge cell comprised a hollow anode (3 mm bore) and a hollow cathode (3 mm bore) with electrodes made of Mo, Ta, W, Al, or Mg (see Figure 1). The electrodes were separated by a 3 mm gap. A high voltage DC power supply was used to charge a bank of twenty 5200 pF capacitors connected in parallel to the electrodes. The cathode was maintained at a voltage of -10 kV before the triggering, while the anode was grounded. In some experiments, the voltage was increased up to -15 kV and decreased to -7 kV to determine the influence of this parameter on the observed spectra. An electron gun (Clinton Displays, Part # 2-001), driven by a high voltage pulse generator (DEI, PVX 4140), provided a pulsed electron beam with electron energy of 1–3 keV and pulse duration of 0.5 ms. The electron-beam triggered a high voltage pulsed discharge at a repetition rate of 5 Hz. The discharge was also self-triggered to determine the influence of the electron-beam on the spectral emission, and the electron-beam triggered repetition rate was varied between 1 Hz and 5 Hz to determine if the electrode metal was the source of the continuum by varying the electrode temperature and vaporization rate.

The discharge cell was aligned with the spectrometer using a laser. The CCD detector was gated synchronously with the e-beam trigger. It had an exposure time of 100 ms for each discharge pulse having a breakdown time of about 300 ns. Each recorded spectrum accumulated radiation from 500 or 1000 discharges and in one case 5000 discharges. The CCD dark count was subtracted from the accumulated spectrum. The wavelength calibration was confirmed by O V and O VI lines from the oxygen present on the electrodes in the form of metal oxides. Radiation was measured through an aperture that limited the gas flow from the discharge chamber into the detector chamber. Two-stage differential pumping resulted in low gas pressure in the detector chamber (in the range of 1×10^{-6} Torr) while the gas pressure in the discharge chamber was maintained in the range from 0.1 Torr to 1.3 Torr. Typical flow rates of ultrahigh purity helium, hydrogen, and mixtures ranged from 1 sccm to 10 sccm, and the pressure in the discharge chamber was controlled by a mass flow controller (MKS). Both on-line mass spectroscopy and visible spectroscopy were used for monitoring contaminants in the plasma forming gases.

The pure hydrogen EUV spectra were recorded using an Aluminum (Al) (150 nm thickness, Luxel Corporation) filter to demonstrate that the soft X-rays are emitted from the plasma. The CCD detector position in the beam dispersed by the grating was changed from being centered at 20 nm to 10 nm to determine the short-wavelength cutoff of the hydrogen continuum radiation at about 10 nm using the 600 g/mm grating and Ta electrodes.

3. 2 EUV spectra of ignited solid fuels and spectroscopic measurement of the EUV optical power balance

EUV spectroscopy (Figure 3) under differentially-pumped vacuum conditions was performed on solid fuel samples comprising (i) a 0.08 cm^2 nickel screen conductor coated with a thin (<1 mm thick) tape cast coating of NiOOH, 11 wt % carbon, and 27 wt% Ni powder, (ii) 40 mg of Ag (87 wt%) + BaI_2 $2H_2O$ (13 wt%), (iii) 5 mg energetic material NH_4NO_3 sealed in an aluminum DSC pan (75 mg) (aluminum crucible 30 µl, D: 6.7 mm×3 mm (Setaram, S08/HBB37408) and aluminum cover D: 6.7 mm, stamped, tight (Setaram, S08/HBB37409)) (DSC pan), (iv) 5 mg energetic material gun powder sealed in the Al DSC pan, and (v) 30 mg paraffin wax sealed in the DSC pan.

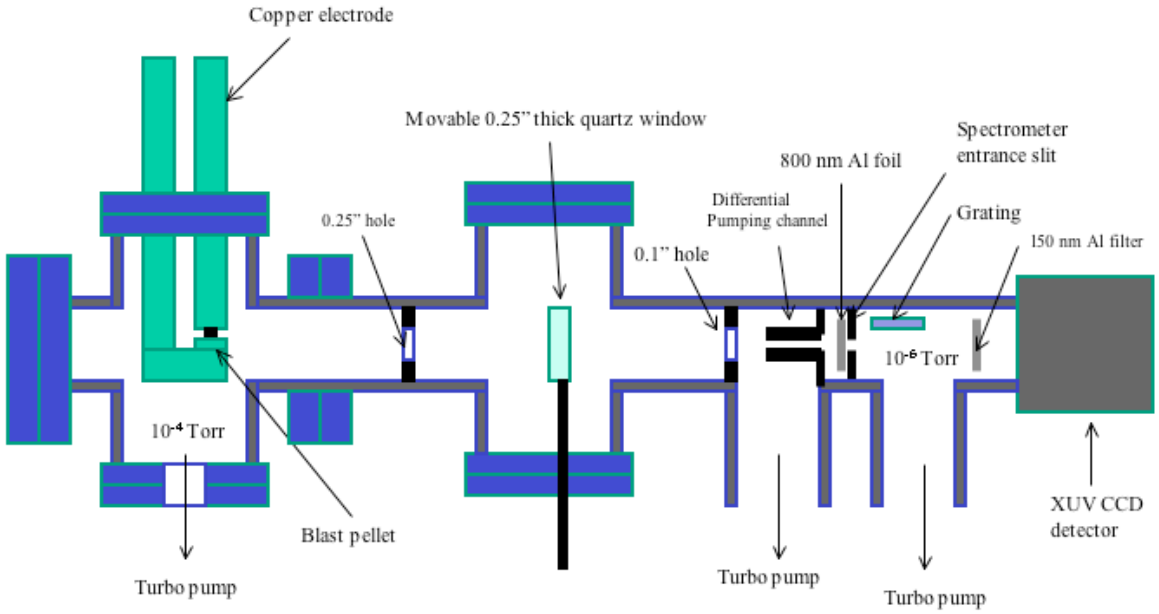

Figure 3. Experimental setup for the ignition of conductive solid fuel samples and the recording of the intense plasma emission. The plasma expands into a vacuum chamber such that it becomes optically thin. The source emits its light spectrum through an entrance aperture passing through a slit, with the spectrum dispersed off a grazing-incidence grating onto a CCD detection system.

Each sample was contained in a vacuum chamber evacuated to 5×10^{-4} Torr. The material was confined between the two copper electrodes of a spot welder (Taylor-Winfield model ND-24-75 spot welder, 75 kVA) such that the horizontal plane of the sample was aligned with the optics of an EUV spectrometer as confirmed by an alignment laser. The electrodes were beveled to allow for a larger solid angle of light emission for the Ag (87 wt%) + BaI_2 $2H_2O$ pellet. The sample was subjected to a short burst of low voltage, high current electrical energy. The applied 60 Hz AC voltage was less than 15 V peak, and the peak current was about 10,000–25,000 A. The high current caused the sample to ignite as brilliant light-emitting expanding plasma of near atmospheric pressure. To cause the plasma to become optically thin such that EUV light could emerge, the ignition occurred in a 12 liter vacuum chamber that housed the ignited sample. The pressure in the chamber was 1×10^{-4} Torr. The EUV spectrum was recorded using a McPherson

grazing incidence EUV spectrometer (Model 248/310G) equipped with a platinum-coated 600 g/mm grating. The angle of incidence was 87°. The wavelength resolution with an entrance slit width of 100 μm was about 0.15 nm at the CCD center and 0.5 nm at the limits of the CCD wavelength range window of 50 nm. Two aluminum filters (Luxel Corporation) were placed in the light path to block the intense visible light and to prevent damage to the spectrometer from the blast debris. The transmittance of each Al filter has a transmission window between 17 nm to 80 nm as shown in Figure 4(A). The first 800 nm thick Al filter was placed in front of the entrance slit of the spectrometer, and the second 150 nm thick Al filter was placed between the grating and CCD detector. To search for the 10.1 nm short wavelength cutoff of the H(1/4) transition continuum radiation while selectively blocking visible light, a 150 nm thick Zr filter (Luxel Corporation) was placed in the light path between the grating and CCD detector. The transmittance of the Zr filter has a transmission window in the region of 10 nm as shown in Figure 4(B). The distance from ignited solid fuel sample plasma source to the spectrometer entrance was 75 cm. The EUV light was detected by a CCD detector (Andor iDus) cooled to -60 °C. The CCD detector was centered at 20 nm, and the wavelength region covered was 0 to 45 nm. Known oxygen and nitrogen ion lines observed in a high voltage pulse discharge spectrum were used to calibrate the wavelengths of the 0 to 45 nm region. A calibration spectrum was obtained on a high voltage discharge in air plasma gas at 100 mTorr using W electrodes.

LUXEL CORPORATION

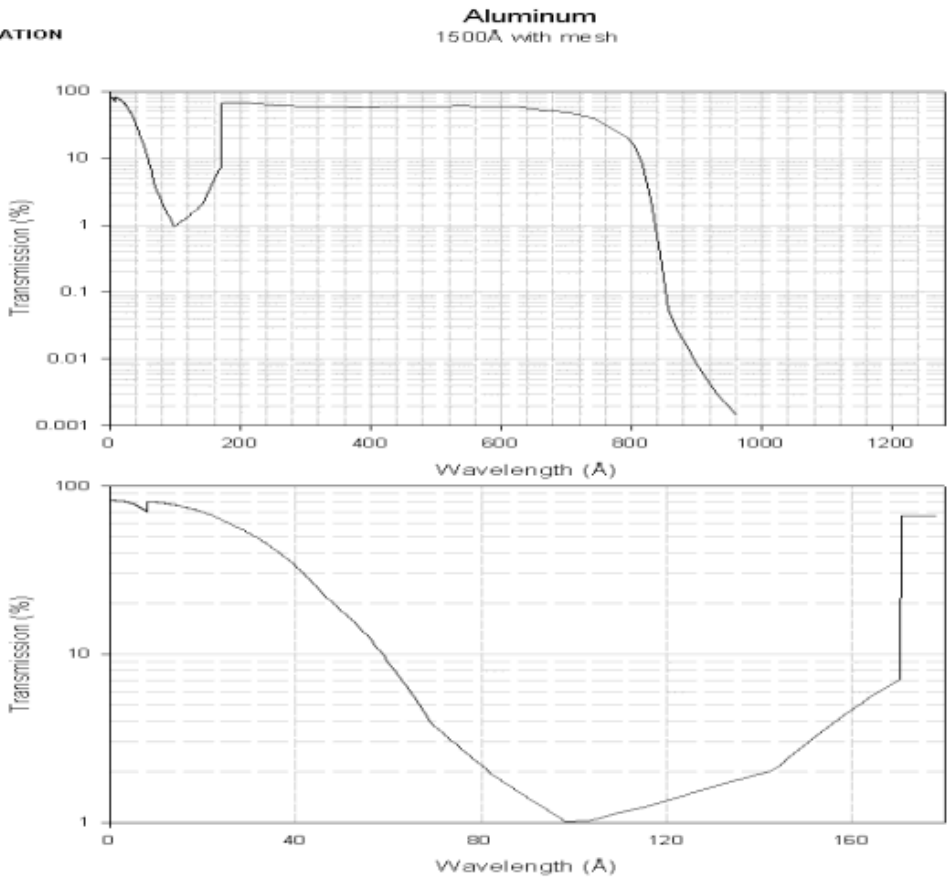

(A)

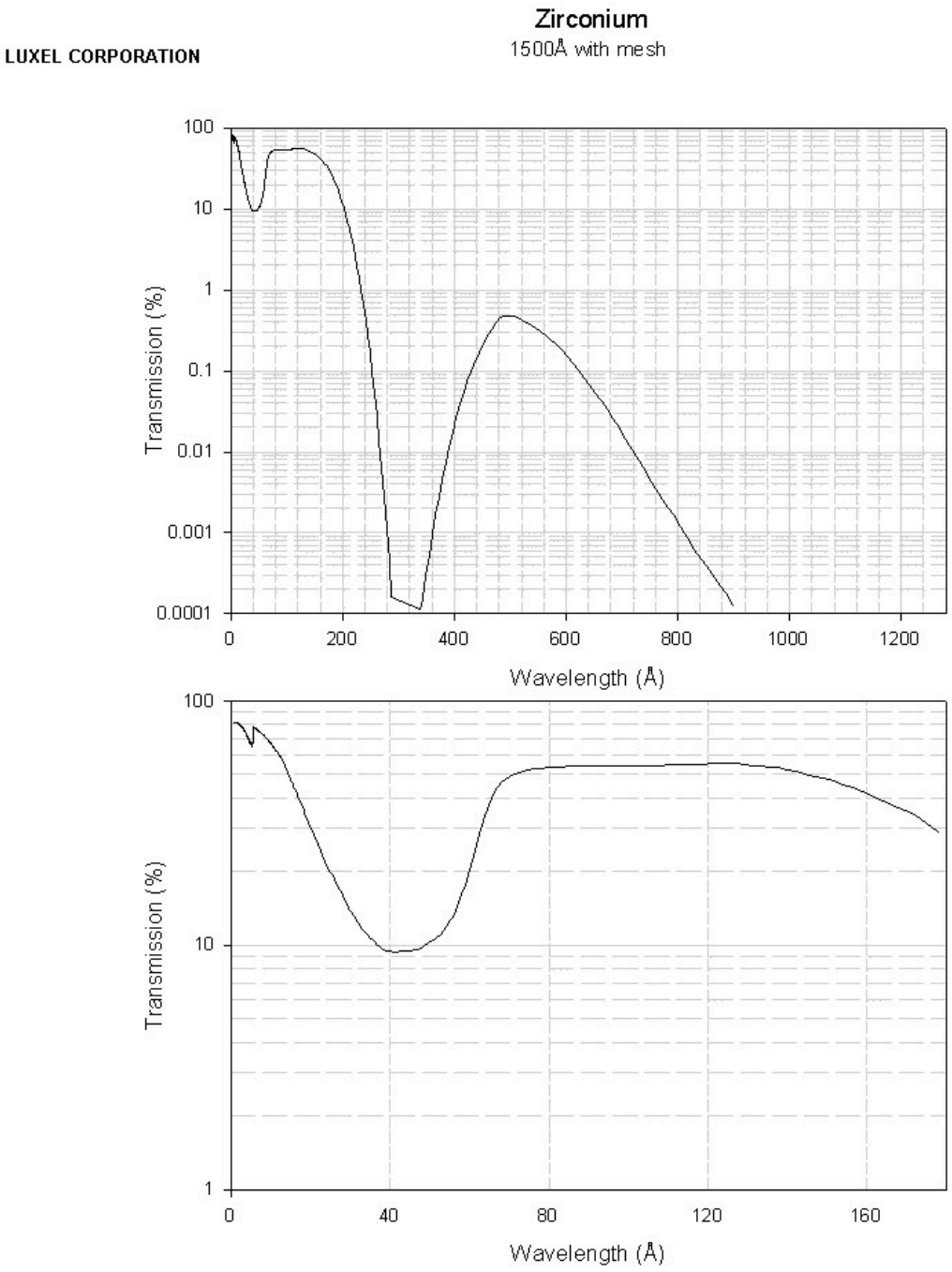

(B)

Figure 4. Transmission curves of filters for EUV light that blocked visible light. (A) The Al filter (150 nm thickness) having a cutoff to short wavelengths at ~17 nm. (B) The Zr filter (150 nm

thickness) having high transmission at the predicted H(1/4) transition cutoff 10.1 nm.

The hydrogen pinch plasma formed by the methods and systems of section 3.1 served as a standard light source of known incident radiation energy determined by an efficiency calculation of the energy stored in the capacitors to light with the emission treated as a point source. The incident energy was corrected for distance and solid angle to give the energy density of the H_2 pinch plasma at the slits. Using the slit dimensions, the photon energy passing through the 50 μm slits was calculated. Correcting for the grating efficiency for EUV of 15%, the CCD quantum efficiency (QE) for EUV of 90%, the Al filter transmission rate (0.15 μm Al foil) of 80%, and the Al filter transmission rate (0.8 μm Al foil) of 15% gave the calculated detection energy. The total EUV photon counts of the calibration H_2 pinch plasma spectrum was measured (section 3.1). Using the average photon wavelength of 40 nm wherein the Al filter has a band pass from 17 nm to 80 nm, the corresponding measured or observed energy was calculated. The ratio of the calculated and observed energy gave the calibration factor that accounts for other inefficiencies in the detection. The reverse application of the photon energy at the average wavelength of 40 nm and the correction factors applied to the total EUV photon counts of the solid fuel allowed for the calculation of the corresponding incident radiation energy.

3.3 Ignition of H_2O-based solid fuels with a low voltage, high current and plasma duration determination

Test samples comprised (i) H_2O-based solid fuels 100 mg Cu + 30 mg H_2O (All metal samples comprised powder. H_2O was deionzed) sealed in the DSC pan, 80 mg Ti + 30 mg H_2O sealed in the DSC pan, a 1 cm^2 nickel screen conductor coated with a thin (<1 mm thick) tape cast coating of NiOOH, 11 wt % carbon, and 27 wt% Ni powder, and 55.9 mg Ag (10 at%) coated on Cu (87 wt%) + BaI_2 $2H_2O$ (13 wt%), (ii) hydrocarbon-based solid fuel paraffin wax sealed in the DSC pan, (iii) control H_2O-based reaction mixtures 185 mg In + 30 mg $CaCl_2$ + 15 mg H_2O, 185 mg In + 30 mg $ZnCl_2$ + 15 mg H_2O, 185 mg Bi + 30 mg $ZnCl_2$ + 5 mg H_2O, and 185 mg Sn + 30 mg $ZnCl_2$ + 5 mg H_2O, that were not catalytic to form hydrinos, and (iv) control conductive materials not comprising H_2O such as pre-dehydrated metal foils and a 0.0254 cm diameter gold wire loop and a 2.38 mm diameter InSn wire loop wherein each wire was oriented for axial current flow and was preheated in vacuum. The samples were loaded into the electrodes of the Acme 75 kVA welder that was activated to apply high current through each under atmospheric pressure argon. The AC current was typically in the range of 10,000–30,000 A, and the peak voltage was typically less than 6 V with the exception of the wire samples having much lower current due to the low voltage and relatively high resistance.

The temporal evolution of the H_2O-based solid fuels such as Cu + H_2O and Ti + H_2O, and hydrocarbon-based solid fuel paraffin wax, all sealed in the DSC pan was measured with a photodiode (Thorlabs, model SM05PD1A) having a spectral range of 350–1100 nm, a peak sensitive wavelength of 980 nm, an active area of 13 mm^2, a rise/fall time of 10 ns, and a junction capacitance of 24 pF at 20 V. The signal was amplified using an amplifier (Opto Diode model PA 100) with a gain of 1× and a 10 V bias and recorded with a 60 MHz scope (Pico Technology, Picoscope 5442B) at a scan interval of 25 ns. The measuring distance was 25 cm. The temporal resolution of the photodiode was confirmed to be within specification by recording the response to a light-emitting diode powered by pulses of 1 μs, 10 μs, and 1 ms that were generated by a function generator (Agilent 33220A 20 MHz Arbitrary Waveform Generator). In each case, a square wave of the width of the temporal width of the pulse was observed.

The expanding plasmas formed from solid fuel ignitions in air were recorded with a Phantom v7.3 high-speed video camera at a rate between 6500 and 150,000 frames per second. Using a ruler in the video background, the expansion velocity of the plasma was determined from the increase in distance between the frames and the time interval between frames. The velocity of the expansion of the plasma front following ignition of the solid fuel 100 mg Cu + 30 mg H_2O sealed in the DSC pan was also measured with a pair of spatially separated conductivity probes. The first probe was 2.54 cm from the origin, and the second was 1.5875 cm more radial relative to the first. Each probe comprised two copper wires separated by 1.27 cm with a 300 V bias applied across the initially open circuit. The ground wire of the wire pair of each probe had a terminal 100 Ohm resistor. The resistor had floating 10× scope probes connected across it to measure the conductivity as a function of time using a scope that measured the voltage through the scope probes. A 10 ns time scale was achieved using a 60 MHz scope (Pico Technology, Picoscope 5442B) with 125 MS/s. The scope trigger voltage was 3 V.

The plasma emission of a solid fuel pellet comprising 55.9 mg of Ag(Cu) (87 wt%) + BaI_2 $2H_2O$ (13 wt%) was synchronously recorded at 17,791 frames per second with the corresponding power parameters as a function of time to determine the relationship of the optical power from the ignited fuel and the input power. The sample chamber was purged with argon and filled with an atmosphere of krypton. The camera used was a Color Edgertronic, and the current and voltage traces as a function of time were recorded at a time resolution of 12 μs per sample using a data acquisition system (DAS) comprising a PC with a National Instruments USB-6210 data acquisition module and Labview VI. A Rogowski coil (Model CWT600LF with a 700 mm cable) that was accurate to 0.3% was used as the current signal source, and a voltage attenuator was used to bring analog input voltage to within the +/-10V range of the USB-6210. Additionally, a Picoscope 5442B was used to also monitor the voltage signal at a time resolution of 208 ns per sample, the same rate as the current.

The visible spectrum over the wavelength region of 350 nm to 1000 nm was recorded using an Ocean Optics visible spectrometer coupled with a fiber optic cable (Ocean Optics Jaz, with ILX511b detector, OFLV-3 filter, L2 lens, 5 μm slit, 350–1000 nm).

3. 4 Spectroscopic measurement of the visible optical power balance

The samples of solid fuel comprising 80 mg Ti + 30 mg H_2O sealed in the Al DSC pan, a 1 cm^2 nickel screen conductor coated with a thin (<1 mm thick) tape cast coating of NiOOH, 11 wt % carbon, and 27 wt% Ni powder, and 5 mg energetic material NH_4NO_3 sealed in the Al DSC pan were ignited in atmospheric pressure argon with an applied peak 60 Hz voltage of 3–6 V and a peak current of about 10,000–25,000 A. The visible power density and energy density spectra were recorded with the Ocean Optics visible spectrometer. The spectrometer was calibrated for optical power density using a standard light source of an Ocean Optics HL-2000 and a radiometer (Dr. Meter Model SM206). To ensure that the short time duration light pulse of the solid fuel was recorded, the calibrated spectrometer was used to record and time-integrate the power density spectrum of the ignited solid fuel over a duration of 5 s, much longer than the light pulse duration of under 1 ms. Background lights were off during recording. Despite the actual acquisition time being short, the distance of recording was 353.6 cm from the origin of the blast to avoid saturation due to the orders of magnitude greater plasma emission intensity than that of a conventional lamp. The total energy density, determined by integrating the energy density spectrum over the wavelength range, was divided by the measured pulse duration time and corrected for the recording distance. The distance was taken as the average spherical radius due to expansion of the plasma calculated from the measured expansion velocity and the time duration of the light event, both measured by the methods of section 3.3.

3. 5 Measurement of the pressure developed from the detonation of solid fuels

The peak side-on overpressures developed with the detonation of solid fuels comprising 30 mg H_2O sealed in the DSC pan, 100 mg Cu + 30 mg H_2O sealed in the DSC pan, and 80 mg Ti + 30 mg H_2O sealed in the DSC pan were measured using a PCB Piezotronics model 137B23B ICP quartz blast pressure sensor with a PCB Piezotronics model 482C05 four-channel ICP sensor signal conditioner. The full scale of the quartz sensor was 50 PSIg. The linearity was 0.10% full scale (0.05 PSIg). The uncertainty was +/- 1% to within a 95% confidence level, and the resolution was 10 mPSIg. The sensor was NIST traceable calibrated. The signal was recorded by a data acquisition system such as a National Instruments USB-6210 module at a sample rate of up to 250 kS/s or a Picoscope 5442B digital oscilloscope at a sample rate of up to 125 MS/s. The quartz blast sensor was positioned at a distance of 33 cm away from the origin of the blast.

3.6 Balmer α line broadening measurements

The width of the 656.3 nm Balmer α line emitted from plasmas of ignited solid fuels 100 mg Cu + 30 mg H_2O and 80 mg Ti + 30 mg H_2O, both sealed in the DSC pan were recorded to determine the electron density. The plasma emission was fiber-optically coupled to a Jobin Yvon Horiba 1250 M spectrometer through a high quality UV (200–800 nm) fiber-optic cable. The spectrometer had a 1250 mm focal length with a 2400 g/mm grating and a detector comprising a Symphony model, liquid-nitrogen cooled, back illuminated 2048×512 CCD array with an element size of 13.5 μm×13.5 μm. The spectrometer resolution was determined by using the 632.8 nm HeNe laser line with the entrance and exit slits set to 20 μm. Background lights were off during recording.

3.7 LED power balance of SF-CIHT cell having photovoltaic conversion

A series of ignitions was performed in air on solid fuel pellets each comprising 80 mg Ti + 30 mg H_2O sealed in the DSC pan. The pellets were adhered to a copper metal strip at 1.9 cm spacing, and the strip was formed around the roller disk of a National Electric Welding Machines seam welder (100 kVA Model #100AOPT SPCT 24) and ignited with an applied peak 60 Hz AC voltage of about 4–8 V and a peak current of about 10,000–35,000 A. The rotation speed was adjusted such that the detonations occurred when the roller moved each pellet to the top-dead center position of the seam welder at a detonation frequency of about 1 Hz. The brilliant flashes of white light were converted into electricity with a photovoltaic converter, and the electricity was dissipated in a light-emitting diode (LED) array.

A three-sided metal frame with attached Lexan walls was setup around the seam welder disks such that the nearest separation of the walls of the rectangular enclosure from the welder disks was about 20 cm. A 30 W, 12 V solar panel was attached to each of the three walls of the enclosure. Each panel comprised high efficiency polycrystalline silicon cells, low iron tempered glass and EVA film with TPT back sheet to encapsulated cells with an anodized aluminum alloy frame (Type 6063-T5 UL Solar). Other solar panel specifications were: cell (polycrystalline silicon): 15.6 cm×3.9 cm; number of cells and connections: 36 (4×9); dimension of module: 66.6×41.1×2.50 cm^3; weight: 3.63 kg. The electrical characteristics were: power at STC: 30 W; maximum power voltage (V_{pm}): 17.3 V; maximum power current (I_{pm}): 1.77 A; open circuit voltage (V_{oc}): 21.9 V; short circuit current (I_{sc}): 1.93 A; tolerance: ±5%; standard test conditions: temperature 25 °C, irradiance 1000 W/m^2, AM = 1.5; maximum system voltage: 600 V DC; series fuse rating: 10 A; temperature coefficient I_{sc}: 0.06%/K, V_{oc}: -0.36%/K, P_{max}: -0.5%/K; operating temperature: -40 °C to +85 °C; storage humidity: 90%; type of output terminal: junction box; cable: 300 cm.

The solar panels were connected to an LED array. The LED array comprised a Genssi LED Off Road 4×4 Work Light Waterproof 27 W, 12 V, 6000 K (30 Degree Spot), an LEDwholesalers 5 m Flexible LED Light Strip with 300xSMD3528 and Adhesive Back, 12 V, White, 2026WH (24 W total), and a 9 W, 12 V Underwater LED Light Landscape Fountain Pond Lamp Bulb White. The total estimated power output at the rated voltage and wattage of the LEDs was 27 W + 24 W + 9 W = 60 W. The collective output power of the three solar panels was 90 W under 1 Sun steady state conditions.

4. Basic experimental results and discussion

4.1 EUV pinch plasma spectra

The reported EUV emission spectra [5, 6] of electron-beam-initiated, pinch discharges in pure helium and hydrogen recorded by the EUV grazing incidence spectrometer with Mo, Ta, and W electrodes and different gratings, spectrometers, and numbers of CCD image superpositions are shown in Figures 5(A)–(D).

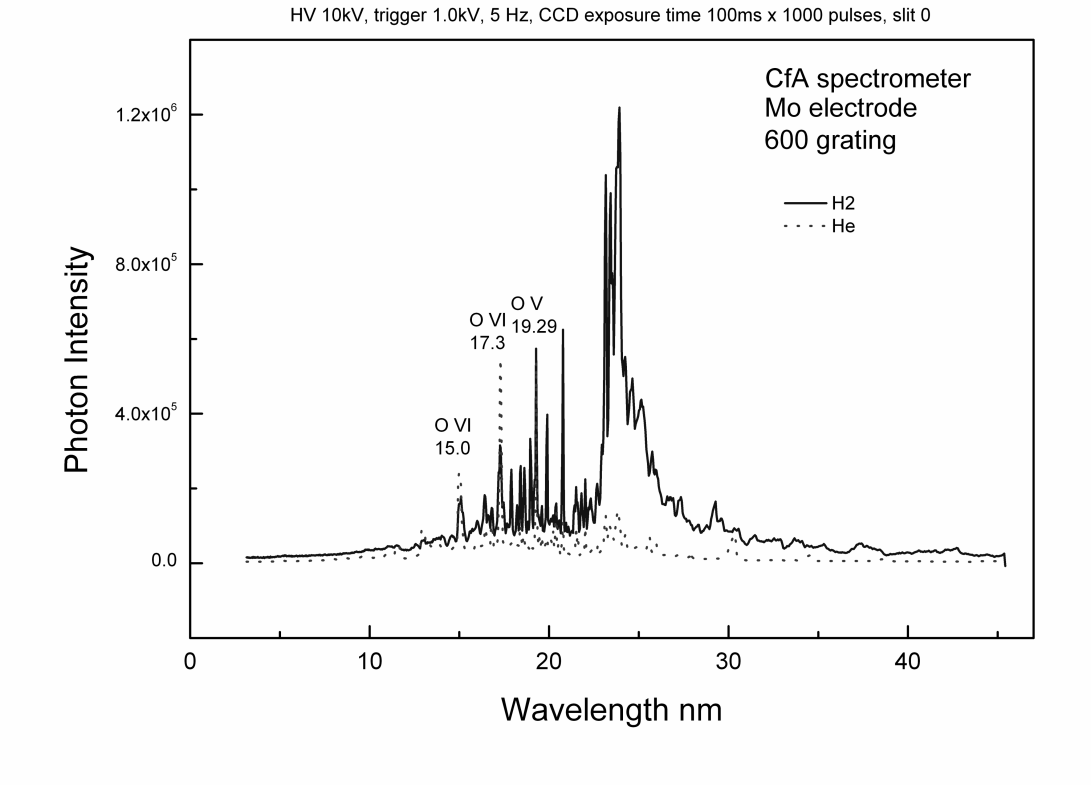

(A)

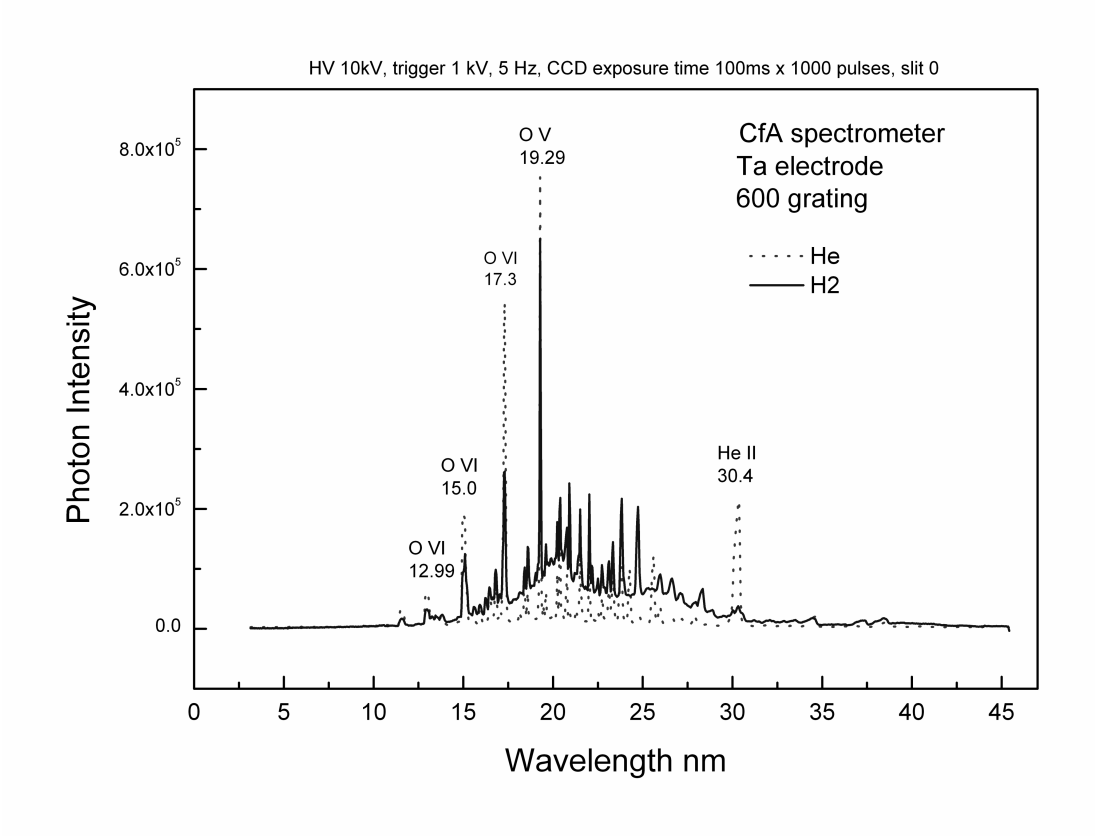
HV 10kV, trigger 1 kV, 5 Hz, CCD exposure time 100ms x 1000 pulses, slit 0
CfA spectrometer
Ta electrode
600 grating
He
H2
O V
19.29
O VI
17.3
O VI
15.0
O VI
12.99
He II
30.4
Photon Intensity
Wavelength nm
8.0x10^5
6.0x10^5
4.0x10^5
2.0x10^5
0.0
0
5
10
15
20
25
30
35
40
45

(B)

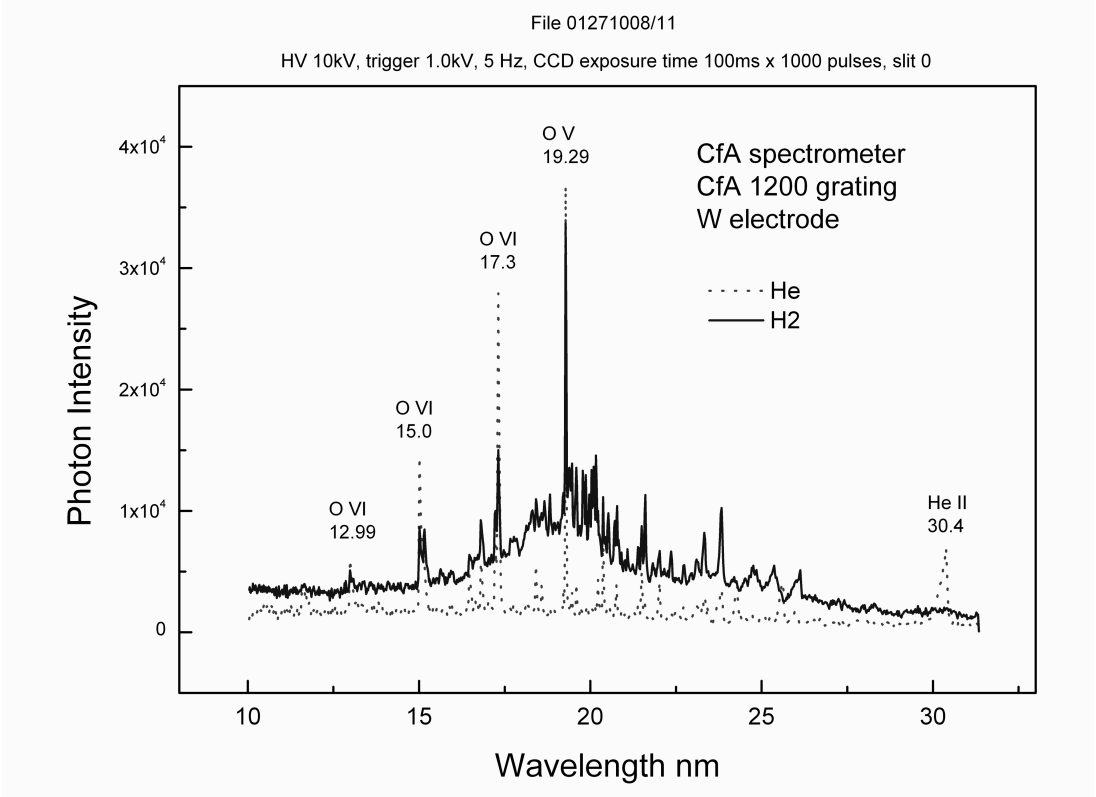
File 01271008/11
HV 10kV, trigger 1.0kV, 5 Hz, CCD exposure time 100ms x 1000 pulses, slit 0
CfA spectrometer
CfA 1200 grating
W electrode
He
H2
O V
19.29
O VI
17.3
O VI
15.0
O VI
12.99
He II
30.4
Photon Intensity
Wavelength nm
4x10^4
3x10^4
2x10^4
1x10^4
0
10
15
20
25
30

(C)

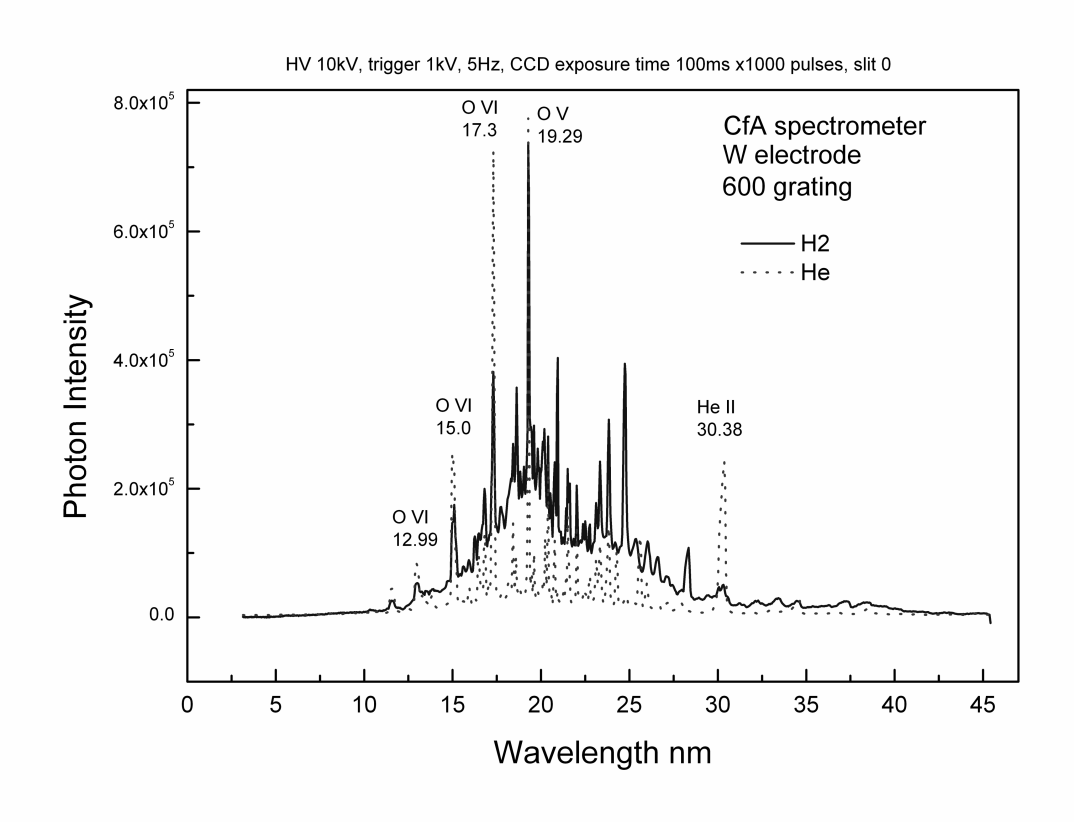

(D)

Figure 5. Emission spectra (2.5–45 nm) comprising 1000 superpositions of electron-beam-initiated, high voltage pulsed gas discharges in helium or hydrogen. Only known helium and oxygen ion lines were observed with helium in the absence of a continuum. Continuum radiation was observed for hydrogen only independent of the electrode, grating, spectrometer, or number of CCD image superpositions. (A) Helium and hydrogen plasmas maintained with Mo electrodes and emission recorded using the CfA EUV grazing incidence spectrometer with the BLP 600 lines/mm grating. (B) Helium and hydrogen plasmas maintained with Ta electrodes and emission recorded using the CfA EUV grazing incidence spectrometer with the BLP 600 lines/mm grating. (C) Helium and hydrogen plasmas maintained with W electrodes and emission recorded using the CfA EUV grazing incidence spectrometer with the CfA 1200 lines/mm grating. (D) Helium and hydrogen plasmas maintained with W electrodes and emission recorded using the CfA EUV grazing incidence spectrometer with the BLP 600 lines/mm grating.

Prior spectra of discharges in high purity helium were measured as reference for validation of the continuum-free spectra in absence of hydrogen [5, 6]. The known helium ion

lines were observed in the absence of any continuum radiation. Oxygen ion lines were also observed similarly in all spectra including those from hydrogen discharges due to the oxide layer on the metal electrodes. In contrast to the helium spectra, the continuum band was observed when pure hydrogen was discharged. Continuum radiation in the 10 nm to 30 nm region was observed from the hydrogen discharge regardless of the electrode material, spectrometer, or grating with the intensity proportional to the hydrogen partial pressure. This dependency of the continuum intensity on the H_2 pressure was also observed in helium-hydrogen mixtures as shown in Figure 6. Conventional mechanisms of the continuum radiation unique to hydrogen in a region wherein hydrogen was previously not known to emit were sought. Considering the low energy of 5.2 J per pulse, the observed radiation in the energy range of about 120 eV to 40 eV, reference experiments and analysis of plasma gases, cryofiltration to remove contaminants, and spectra of the electrode metal, no conventional explanation was found in the prior work to be plausible including contaminants, thermal electrode metal emission, and Bremsstrahlung, ion recombination, molecular or molecular ion band radiation, and instrument artifacts involving radicals and energetic ions reacting at the CCD and H_2 re-radiation at the detector chamber [5, 6].

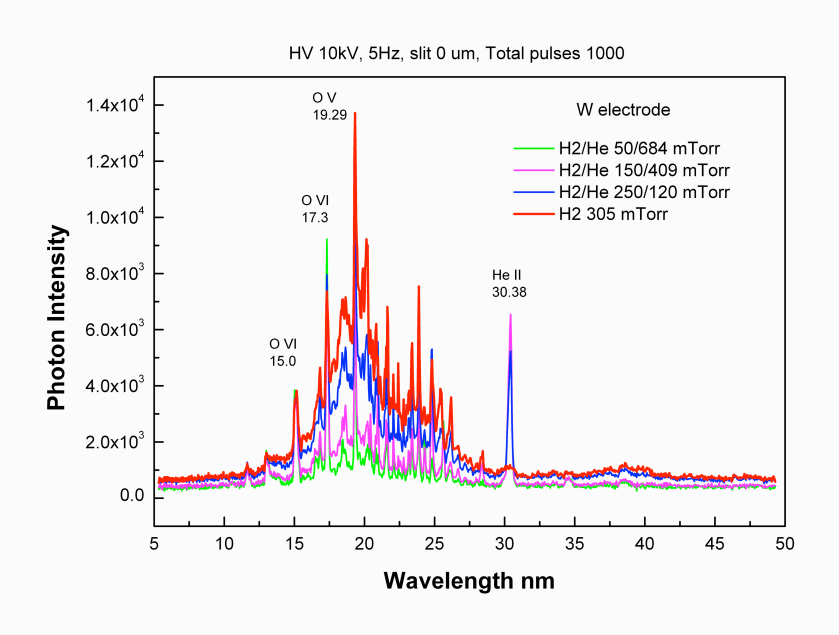

Figure 6. Emission spectra (5–50 nm) of electron-beam-initiated, high voltage pulsed discharges in helium-hydrogen mixtures with W electrodes recorded by the EUV grazing incidence spectrometer using the 600 lines/mm grating and 1000 superpositions showing that the continuum radiation increased in intensity with increasing hydrogen pressure.

Consider the potential catalysts and mechanisms of continuum emission. In H and mixed H plasmas maintained with metal electrodes each having an oxide coat, the primary catalyst candidates are mH and HOH, and both may be active. The energy released with HOH as catalyst is 122.4 eV from H*(1/4) intermediate, and the energy including the HOH catalyst during the transition is 204 eV which could result in emission to 6 nm. Similarly, in hydrogen-helium microwave plasma, H undergoing catalysis with H (m=1) as the catalyst can give rise to a concerted energy exchange of the total energy of 40.8 eV with the excitation of the He ($1s^2$) to He ($1s^1 2p^1$) transition (58.5 nm, 21.21 eV) yielding broad continuum emission with $\lambda \leq 63.3$ nm (≥ 19.59 eV). In independent replication experiments, broad 63.3 nm emission of this nature and the continuum radiation have been observed in helium-hydrogen microwave plasmas and in hydrogen pinch plasmas, respectively [3, 29]. But, $\mathrm{H}*\left[\frac{a_{\mathrm{H}}}{m+1}\right]$ should be the predominant source of continuum radiation since the plasma comprised hydrogen and some oxygen from the electrodes. With mH catalyst, the possibilities for continuum radiation in this range are the 10.1 nm continuum (m=3 in equations (1)–(4) and (9)), and 22.8 nm continuum (m = 2 in equations (1)–(4) and (9)). One piece of evidence against mH as the catalyst is that any 10.1 nm continuum should be dramatically lower in intensity than the emission of the 22.8 nm continuum. In contrast, evidence for the HOH catalyst is that the intensity for the 10.1 nm continuum has been observed to be higher in H pinch plasmas with W and Ta electrodes. This is explained by HOH having a 10.1 nm continuum emission as the source of the 10–30 nm band. Solid fuels comprising metal oxides and hydroxides that undergo hydrogen reduction to form HOH show substantial excess energy [30, 31]. These results as well as those of electrochemical (CIHT) cells utilizing the HOH catalyst [30–32] show that HOH catalyst has much higher kinetics than mH catalyst, and the reaction is favorable with metal oxides such as those of Mo, W, and Ta that favorably undergo hydrogen reduction to form HOH catalyst. The strong oxygen ion lines in the continuum from the H pinch plasma show the presence of metal oxide that is permissive of the HOH mechanism. Conversely, metal oxides that are not thermodynamically favorable towards the reaction to form HOH such as those of Al and Mg shown in Figures 7(A)–(D) do not show the continuum radiation under the low energy conditions of 5 J per pulse corresponding to an electron temperature estimated to be <10 eV of our pinch plasma source.

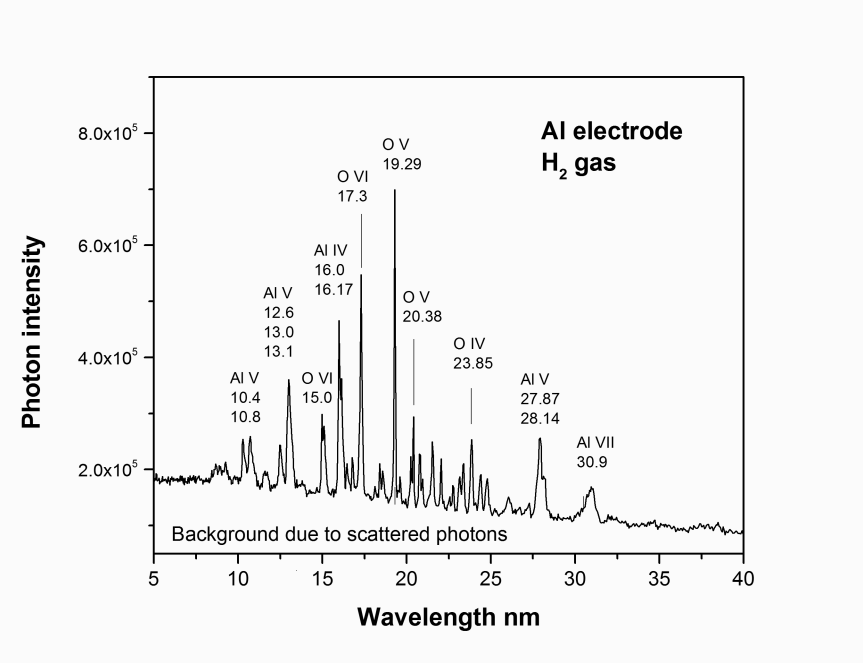
Al electrode
H2 gas
Photon intensity
Wavelength nm
Background due to scattered photons
O V 19.29
O VI 17.3
Al IV 16.0 16.17
Al V 12.6 13.0 13.1
O V 20.38
O IV 23.85
Al V 10.4 10.8
O VI 15.0
Al V 27.87 28.14
Al VII 30.9
8.0x10^5
6.0x10^5
4.0x10^5
2.0x10^5
5
10
15
20
25
30
35
40

(A)

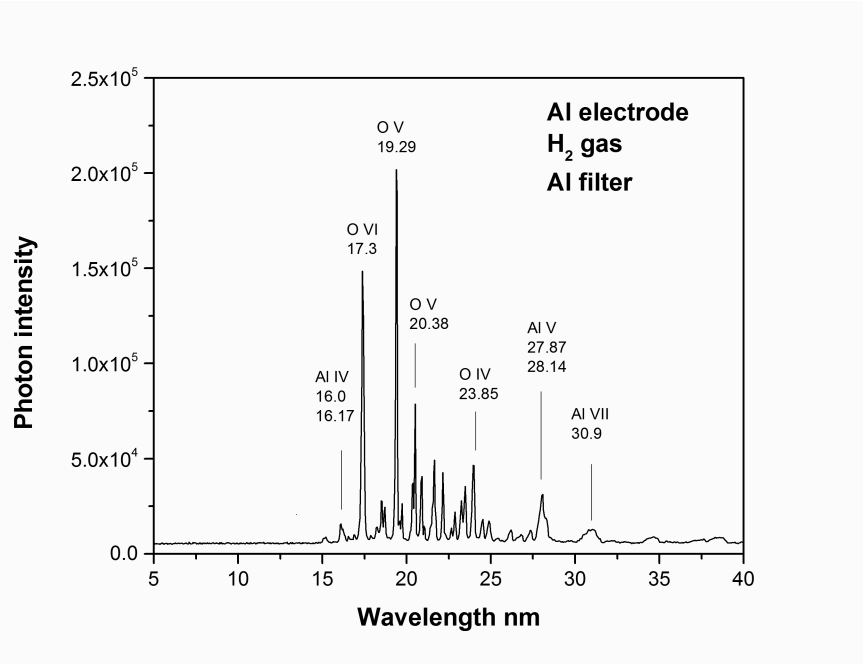
Al electrode
H2 gas
Al filter
Photon intensity
Wavelength nm
O V 19.29
O VI 17.3
O V 20.38
Al V 27.87 28.14
Al IV 16.0 16.17
O IV 23.85
Al VII 30.9
2.5x10^5
2.0x10^5
1.5x10^5
1.0x10^5
5.0x10^4
0.0
5
10
15
20
25
30
35
40

(B)

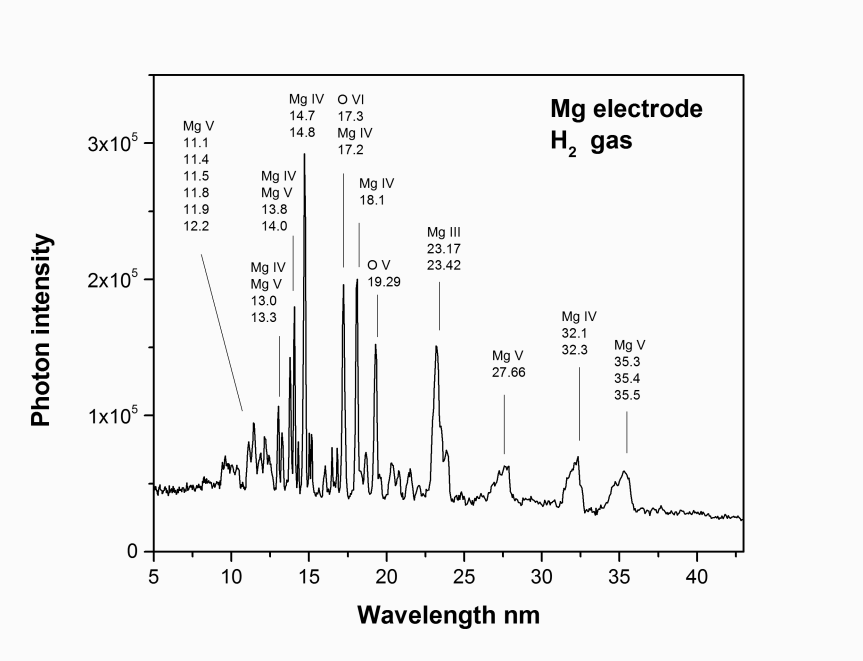

(C)

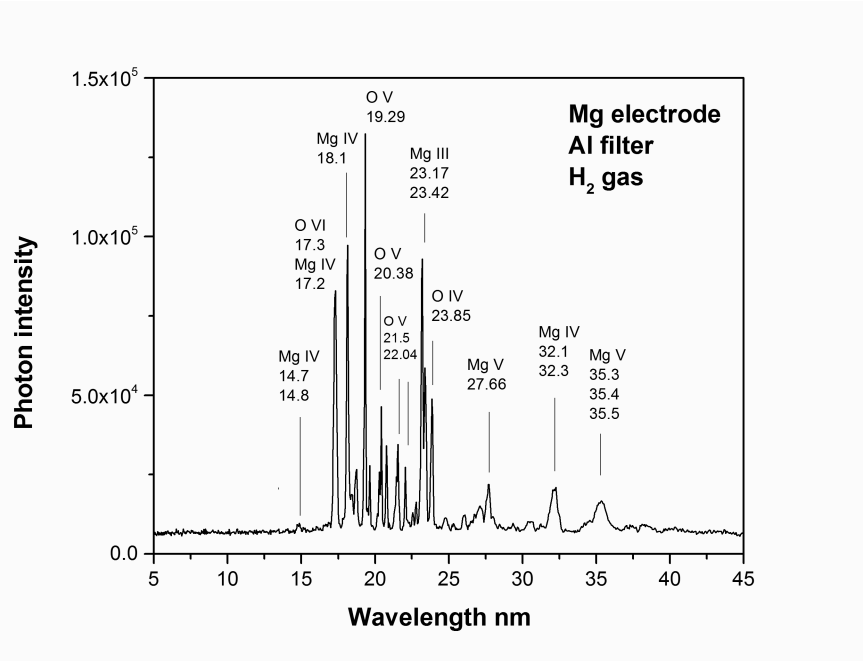

(D)

Figure 7. Emission spectra (5–40 nm) comprising 1000 superpositions of electron-beam-initiated, high voltage pulsed gas discharges in hydrogen with and without an Al filter. No continuum radiation was observed from Al and Mg anodes. (A) Hydrogen plasmas maintained with an Al anode. (B) Hydrogen plasmas maintained with an Al anode with the spectrum

recorded with an Al filter. (C) Hydrogen plasmas maintained with an Mg anode. (D) Hydrogen plasmas maintained with an Mg anode with the spectrum recorded with an Al filter.

All high Z metals emit continuum radiation at a sufficiently high electron temperature. Specifically, it is shown by Awe et al. that Al forms a strong metal ion continuum at much higher energies and electrons temperatures [33]. Any coincidence between the continuum emission of our source and that achieved typically at an electron temperature of over two orders of magnitude higher by other much more powerful sources may be due to secondary emission from absorption of the high-energy continuum radiation by metal atoms to form highly ionized metal ions in the plasma or due to a significant increase in the background emission of ambient species such as low abundance ions by the same mechanism. For example, an electron temperature of 163 eV is required to observe W continuum radiation in the EBIT source [34]. At the very low electron temperature our hydrogen pinch source is estimated to be <10 eV, any highly-ionized ion emission that would otherwise require a much higher electron temperature than the actual temperature must be due to the high energy provided according to equations (1)–(9). This ion emission is of a nonthermal nature as confirmed by the absence of required emission of the lines of these ions and equilibrium species in the visible region [5]. The same mechanism is shown in the solar corona as the basis of nonthermal highly-ionized ion emission as well as ion emission in white dwarf stars in section 4.9. In the latter case, the actual minority-species absorption lines in the continuum background are observed (Figure 22). Thus, the emission is not consistent with the electron temperature in terms of the ions observed and line intensity ratios. Specifically, as shown in reference [5] in the case of a W anode, the very weak atomic W visible emission and low electron temperature do not support the short wavelength continuum being due to highly ionized W ions unless there is a continuum-emission energy source to excite these ions if they are otherwise present in low abundance. This assignment of highly-ionized ion emission is confirmed by the observation of the same type of ion emission from a plasma source that has no high electric field, namely an ignited solid fuel as shown in section 4.6.

In the case that the medium is optically thick over certain wavelength regions, only parts of the broad emission may be observed (Figure 5(A) versus Figures 5(B)–(D). Consequently, the continuum radiation may be indirectly observed as highly-ionized ion emission not consistent with a thermal origin in terms of the ions and intensity ratios. The emission depends on atomic and ion cross sections for absorption and reemission of the continuum radiation as well as the incident continuum profile. The latter is dependent on the hydrino reactions that in turn also depend on the medium wherein a species other than H may serve as the catalyst [3] such as in the case of HOH being the catalyst. Ion emission due to the catalyst reaction such as given in equations (1) and (5) may also be observed. For the involvement of HOH as the catalyst, O ion

afterglow would be expected according to equation (5) wherein the 81.6 eV may give rise to highly ionized oxygen ions. In time-resolved studies using a channel electron multiplier detector and a multichannel scalar counter, the continuum emission was only observed during the short pulse; whereas, oxygen ions showed a long afterglow [29]. For example, the continuum at 25.0 nm had a short lifetime of about 0.5 μs compared to a 4 μs lifetime of the O^{3+} ion line at 23.9 nm. Thus, the observation of O ion lines in the absence of strong metal ion lines was deemed to be due to the long O-ion excited-state lifetimes, excited by the catalysis reaction in addition to absorption and reemission of the EUV continuum. This observation further supports HOH as active in the hydrogen pinch plasma emission. Similarly, helium emission was observed to have a long afterglow with He^+ acting as a catalyst of 54.4 eV ($2 \cdot 27.2$ eV) [4].

Uniquely only hydrogen addition creates or at least greatly enhances the continuum and plasma intensity in the cases wherein HOH catalyst formation is favorable. H addition to a helium pinch plasma decreases the helium ion lifetime; so, H addition should decrease any metal ion continuum; yet, the opposite is observed [4]. The cooling effect by gas admixtures and impurities is reported by Trabert [35]. In contrast, there is no continuum with oxygen, argon, helium, nitrogen, air, or mixtures, for example. The short wavelength radiation in the 10–22 nm region of a Mo anode H_2 pinch plasma did not match conventional plasma models as pointed out by Phelps and Clementson [36] wherein the authors could not exclude a hydrino explanation. The continuum cannot be explained as due to H sputtering as suggested by Phelps and Clementson since H^+ is accelerated towards and bombards the cathode; yet, the continuum is independent of the cathode metal. Furthermore, the explanation of increased electron sputtering on the anode is eliminated since the continuum is observed with trace H present in non-hydrogen plasmas such as essentially pure helium plasma having indistinguishable plasma parameters from 100% helium plasma. This observation also removes an enhanced optical opacity argument regarding diminished transmission of the continuum in helium versus hydrogen. The further observation that there was no continuum from helium even when the light path length between the plasma and the detector was reduced by a factor of one half further eliminated the enhanced optical opacity argument. The hydrino transition is the only viable explanation for all of the results. Moreover, the power released by the hydrino reaction can account for the continuum emission power relative to the EUV emission from the input power based on the H_2 flow rate and availability, energy per transition, and quantum yield for EUV continuum.

Similarly, observed fast H [8–14] may be due to the energy released in forming hydrinos by HOH catalyst, especially in cases such as water vapor plasma where the broadening is greater than 100 eV [10]. HOH may also be a significant contributor in addition to mH catalyst in hydrogen plasma wherein it has been observed that the fast H requires a surface to achieve a significant effect in terms of fractional population and energy [8–14]. For, example, line

broadening is not observed in hydrogen plasma unless a surface such as a metal is present that can support atomic H or HOH formation. Glow discharge and RF discharge cells comprising metal electrodes show a strong effect. Metals typically have an oxide coat, such that the catalyst mechanism may be HOH as well as *m*H. This could explain the large population at very high energies >100 eV in cases with H plasma after long duration running wherein slow accumulation of oxygen is required to yield similar broadening as H_2O plasma. In addition to continuum radiation in the 10–30 nm region and extraordinary fast H as reported previously [5], further confirmation that the energy released by forming hydrinos gives rise to high-kinetic energy H is the ToF-SIMs observation of ions arriving before $m/e = 1$ confirming that the energy release of equations (4) and (8) is manifest as high kinetic energy H^- of about 204 eV [32].

4.2 Ignition of H_2O-based solid fuels with a low voltage, high current and plasma duration determination

The H_2O-based solid fuel samples such as Cu + H_2O sealed in the DSC pan, Ti + H_2O sealed in the DSC pan, and NiOOH + Ni + C as well as control conductive materials not comprising H_2O such as a 0.010" diameter gold wire loop oriented for axial current flow and metal foils preheated in vacuum were loaded into the electrodes of the Acme 75 kVA welder that was activated to apply high current through each sample. Only resistive heating was observed for the controls. Additional H_2O-based reaction mixtures that were not catalytic to form hydrinos and served as controls such as 185 mg In + 30 mg $CaCl_2$ + 15 mg H_2O, 185 mg In + 30 mg $ZnCl_2$ + 15 mg H_2O, 185 mg Bi + 30 mg $ZnCl_2$ + 5 mg H_2O, and 185 mg Sn + 30 mg $ZnCl_2$ + 5 mg H_2O showed just resistive heating behavior as well.

The active H_2O-based solid fuels underwent a detonation event with a loud blast, brilliant light emission, and a pressure shock wave. Each sample appeared to have been completely vaporized and atomized to form an ionized, expanding plasma as evidenced by high-speed video using a Phantom v7.3 camera at 6500 frames per second (Figure 8(A)). With a synchronized recording of the plasma emission at 17,791 frames per second and the corresponding current and voltage as a function of time (Figure 8(B)), the ignition of the solid fuel Ag(Cu) + BaI_2 $2H_2O$ showed that the plasma persisted for 21.9 ms while the input power was zero at 1.275 ms plasma. Plasma having about 100 kW power with no electrical input power and no chemical reaction possible proves the existence of a new energy source shown by EUV spectroscopy (section 4.6) and analytical characterization of the plasma product to be the due to the reaction H to H(1/4).

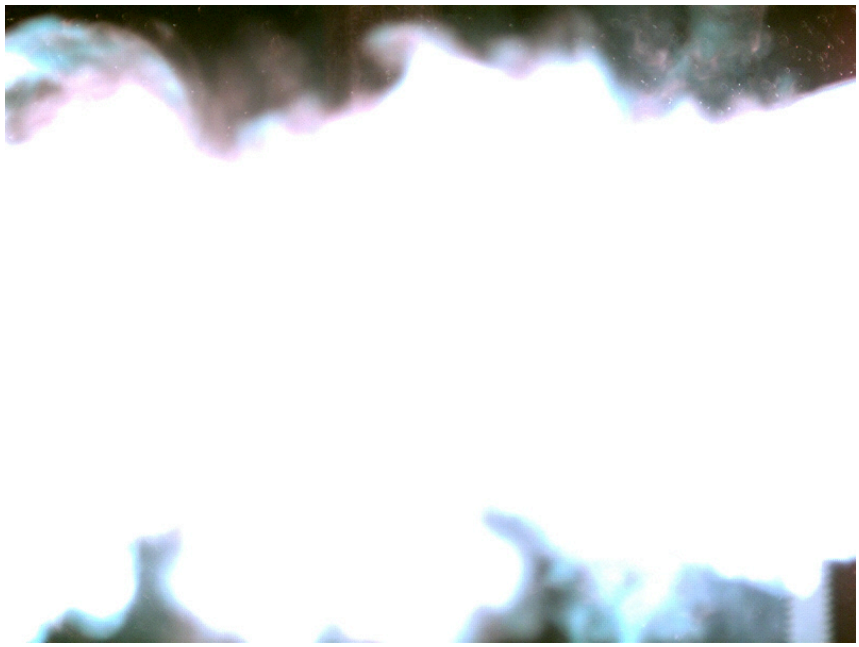

(A)

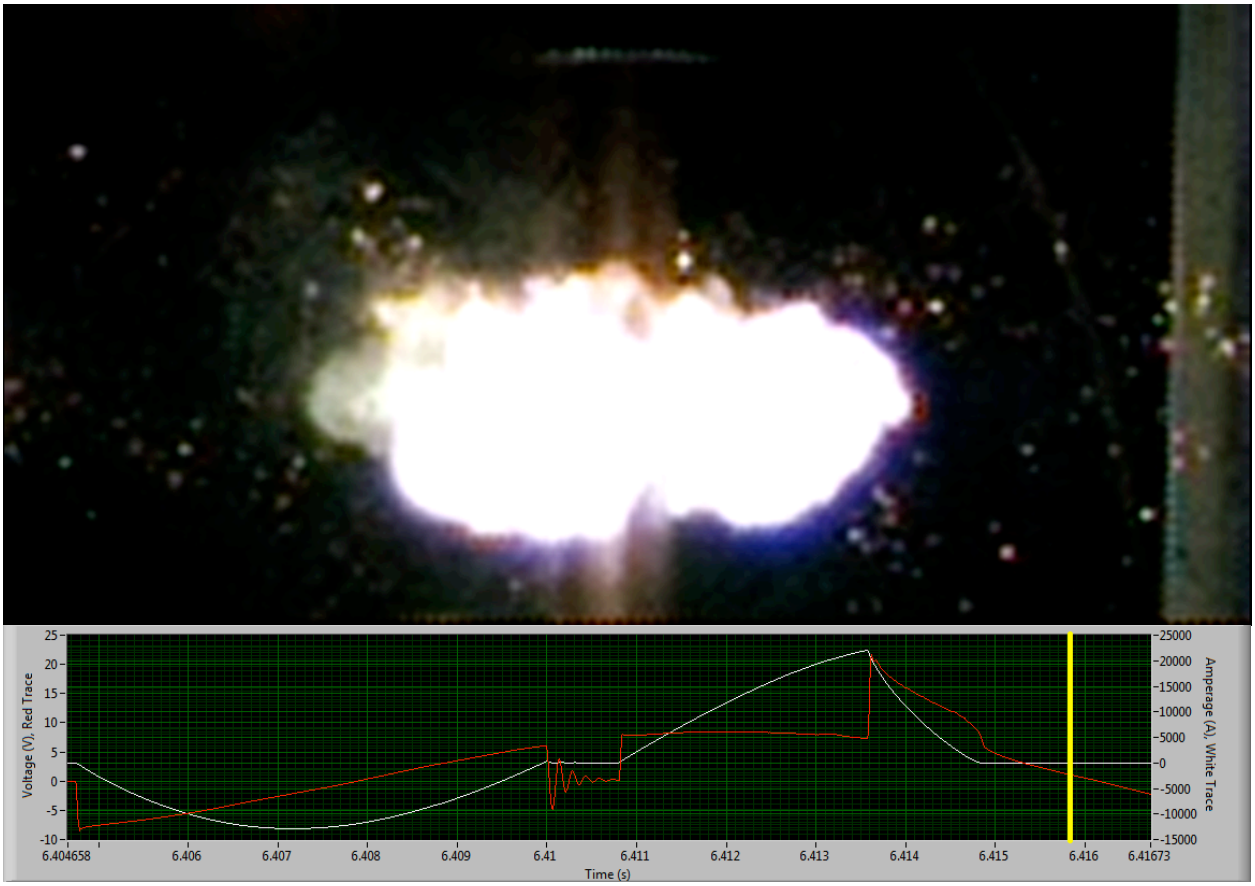
Voltage (V), Red Trace
Amperage (A), White Trace
Time (s)
25
20
15
10
5
0
-5
-10
25000
20000
15000
10000
5000
0
-5000
-10000
-15000
6.404658
6.406
6.407
6.408
6.409
6.41
6.411
6.412
6.413
6.414
6.415
6.416
6.41673

(B)

Figure 8. High-speed photography of brilliant light-emitting expanding plasma formed from the low voltage, high current detonation of the solid fuels. (A) Cu + CuO + H_2O filmed at 6500 frames per second. The white-blue color indicates a large amount of UV emission from a blackbody with a temperature of over 5000 K. (B) 55.9 mg Ag (10 at%) coated on Cu (87 wt%) + BaI_2 $2H_2O$ (13 wt%), filmed at 17,791 frames per second with a VI waveform on the welder arms that shows plasma at a time when there was no electrical input power (noted by the yellow vertical line), and no chemical reaction was possible. The plasma persisted for 21.9 ms while the input power was zero at 1.275 ms. The applied voltage was low, less than 15 V.

The expansion velocity measured from the video at up to 150,000 frames per second was sound speed, 343 m/s, or greater such as 900 m/s. The expansion velocity of the plasma formed by the ignition of solid fuel 100 mg + 30 mg H_2O was also determined to be sound speed by measuring the plasma conductivity as a function of time following detonation of the solid fuel at two spatially separated conductivity probes as shown in Figure 9.

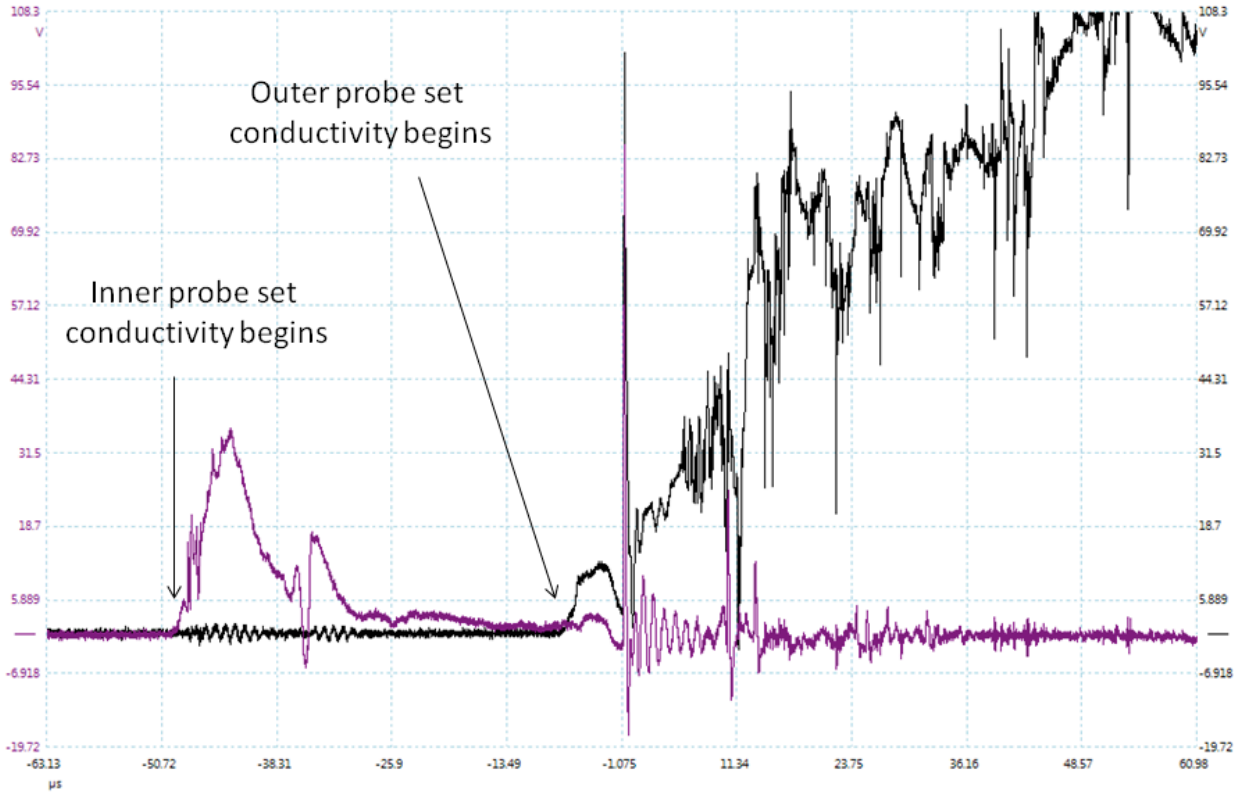

Figure 9. The plasma conductivity as a function of time following detonation of the solid fuel Ti 100 mg + 30 mg H_2O sealed in the DSC pan at a pair of conductivity probes spaced 1.5875 cm apart. The time delay between the pair of conductivity probes was measured to be 42 µs that corresponded to a plasma expansion velocity of 378 m/s which averaged to sound speed, 343

m/s, over multiple measurements.

The brilliant light emission was white in color; the white light being characteristic of the 5000–6000 K blackbody emission of exemplary solid fuels Cu + H_2O and Ti + H_2O shown in Figure 10 compared with the Sun's 5500–6000 K blackbody spectrum. During a phase of the ignition event, the plasma was confirmed to be essentially 100% ionized by measuring the Stark broadening of the H Balmer α line (section 4.4).

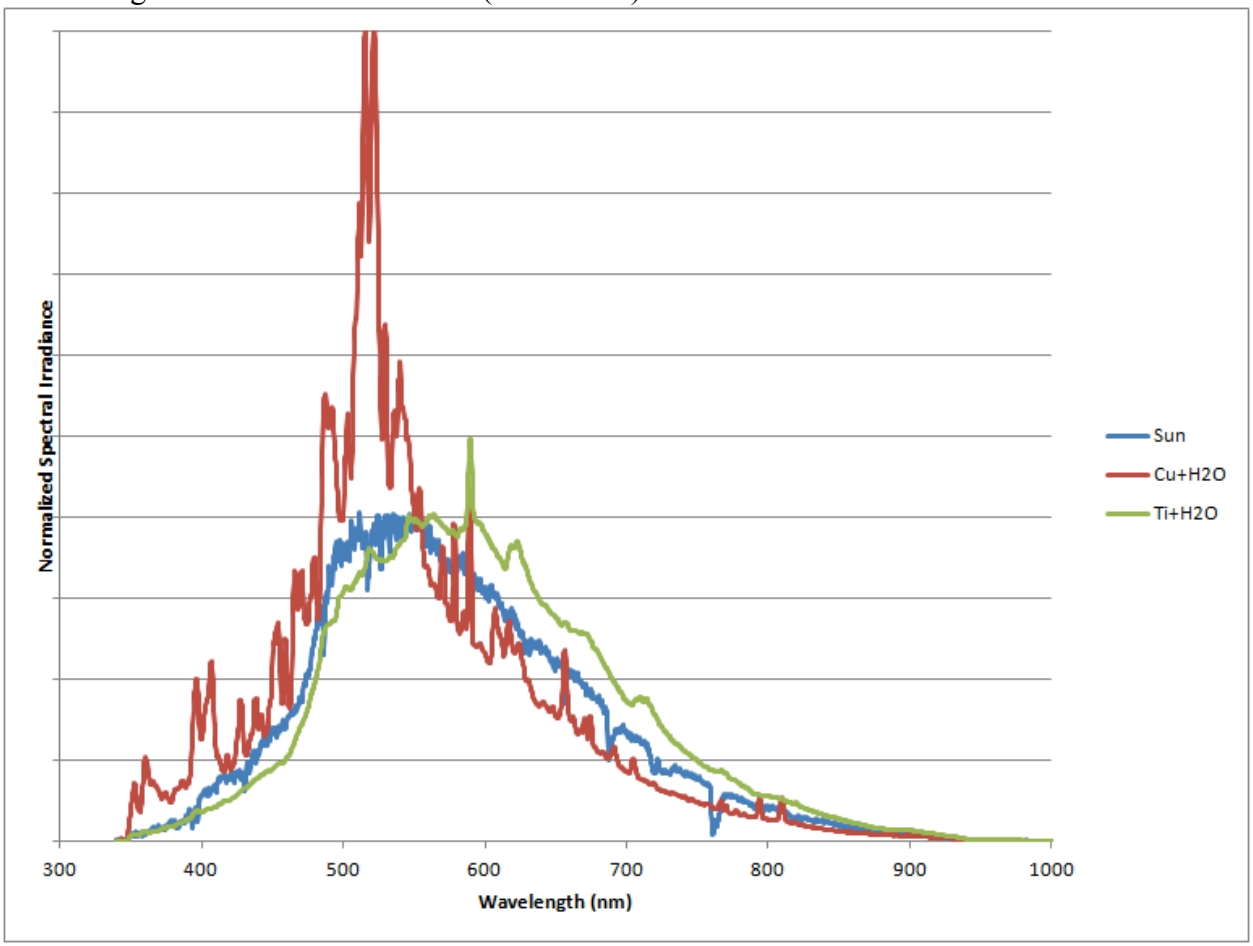

Figure 10. Intensity-normalized, superposition of visible spectra of the plasmas formed by the low voltage, high current ignition of solid fuels 80 mg Ti + 30 mg H_2O and 100 mg Cu + 30 mg H_2O both sealed in the DSC pan, compared with the spectrum of the Sun's radiation at the Earth's surface. The overlay demonstrates that all the sources emit blackbody radiation of about 5000–6000 K, but the solid fuel blackbody emission (before normalization) is over 50,000 times more intense than sunlight at the Earth's surface. Corresponding metal ion emission was also observed from the ignition plasmas.

The photodiode-measured temporal duration of the blast event of exemplary solid fuel 80 mg Ti + 30 mg H_2O sealed in the DSC pan was 0.5 ms (Figure 11). It was observed that the length of the duration of the power generation based on the half-width of the light emission peak could be varied in the range of 25 μs to 40 ms by adjusting the pressure applied to the solid fuel sample by the confining electrodes, the nature of the solid fuel composition, and the waveform of the high current flow through the solid fuel.

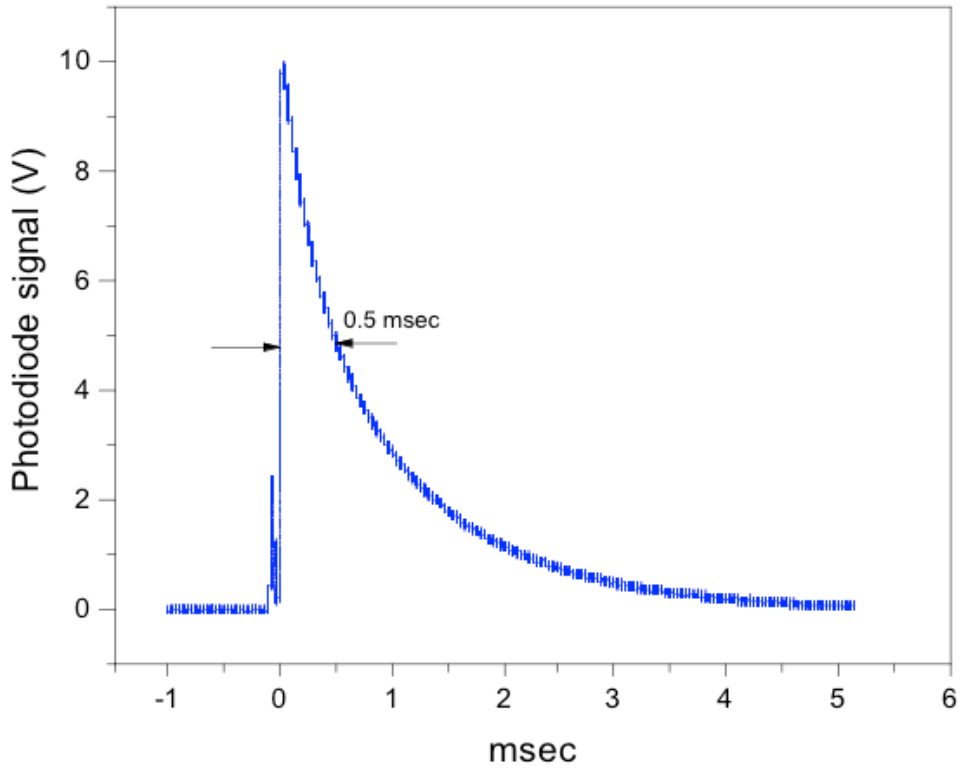

Figure 11. The fast photodiode signal as a function of time capturing the evolution of the light emission following the ignition event of the solid fuel 80 mg Ti + 30 mg H_2O sealed in the DSC pan. The temporal full width half maximum light intensity measured with the fast photodiode was 0.5 ms.

In addition to HOH, *m*H atom catalyst was found to be effective by demonstrating a brilliant light-emitting plasma and blast during the ignition of hydrocarbon-based solid fuel paraffin wax in the DSC pan. As in the case of the H_2O-based solid fuels, blackbody radiation with a temperature of about 5500–6000 K (Figure 12) was observed as shown in Figure 10. Using the fast photodiode, the ignition event was determined to be comprised of two distinct

light-emissions, the first had duration of about 500 µs, and the duration of the second was about 750 µs.

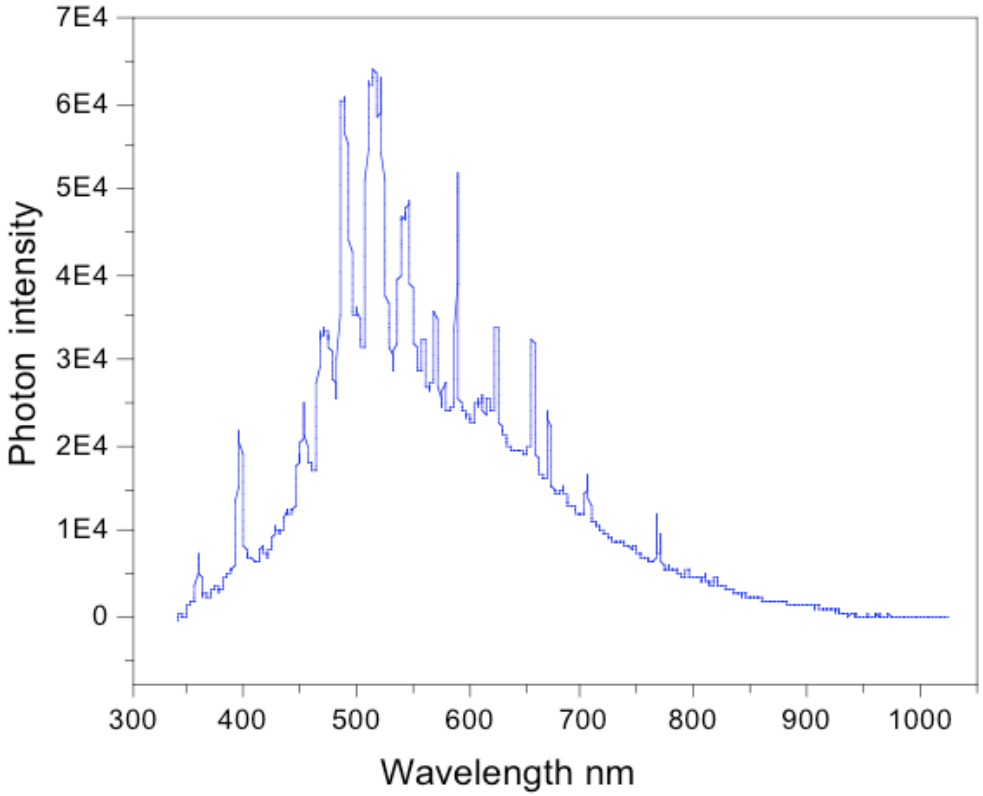

Figure 12. The visible spectrum of the plasma formed by the low voltage, high current ignition of solid fuel paraffin wax sealed in the DSC pan taken at 427 cm from the blast. This source also emits blackbody radiation of about 5000–6000 K similar to the spectra of H_2O-based solid fuels shown in Figure 10.

4. 3 Measurement of the pressure developed from the detonation of solid fuels

With the quartz blast sensor positioned at a distance of 33 cm away from the origin of the blast, the peak side-on overpressures developed from the detonation of 30 mg H_2O sealed in the DSC pan, 100 mg Cu + 30 mg H_2O sealed in the DSC pan, and 80 mg Ti + 30 mg H_2O sealed in the DSC pan were 0.8 PSIg, 1.3 PSIg, and 2.0 PSIg, respectively. The pressure developed by the solid fuels was low compared to that of an internal combustion engine, 735 PSIg [37] and high explosives, 7.35×10^5 PSIg [38, 39]. Thus, the energy of the blast in the form of pressure-volume work is very low. This is consistent with the observation that the solid fuel plasma formed during

a phase of the ignition event was essentially fully ionized. The blackbody temperature was observed to be up to 5500–6000 K. The power was essentially all in the form of radiation.

4.4 Balmer α line broadening measurements

The high resolution, visible spectra in the spectral region of the H Balmer α line measured using the Jobin Yvon Horiba 1250 M spectrometer with 20 μm slits is shown in Figures 13(A) and (B). The full width half maximum (FWHM) of the 632.8 nm HeNe laser line was 0.07 Å that confirmed the high spectral resolution. In contrast, the FWHM of the Balmer α line from the emission of the ignited solid fuel 100 mg Cu + 30 mg H_2O sealed in the DSC pan under atmospheric argon was massively broadened, and the line was shifted by +1.2 Å. The Voigt-fit to the spectral profile gave FWHM of 22.6 Å broadening that is far too excessive to comprise a significant Doppler [8–27] or pressure broadening contribution [40]. An electron density of $4\times10^{23}/m^3$ was determined from the Stark broadening using the formula of Gigosos et al. [41] with the corresponding full width half area of 14 Å. During a phase of the ignition event, the plasma was almost completely ionized. The plasma developed a blackbody temperature of up to about 6000 K. The Balmer α line width from the emission of the ignited solid fuel 80 mg Ti + 30 mg H_2O sealed in the DSC pan could not be measured due to the excessive width, significantly greater than 24 Å, corresponding to a highly ionized plasma. The blackbody temperature was observed to be at least 5000 K.

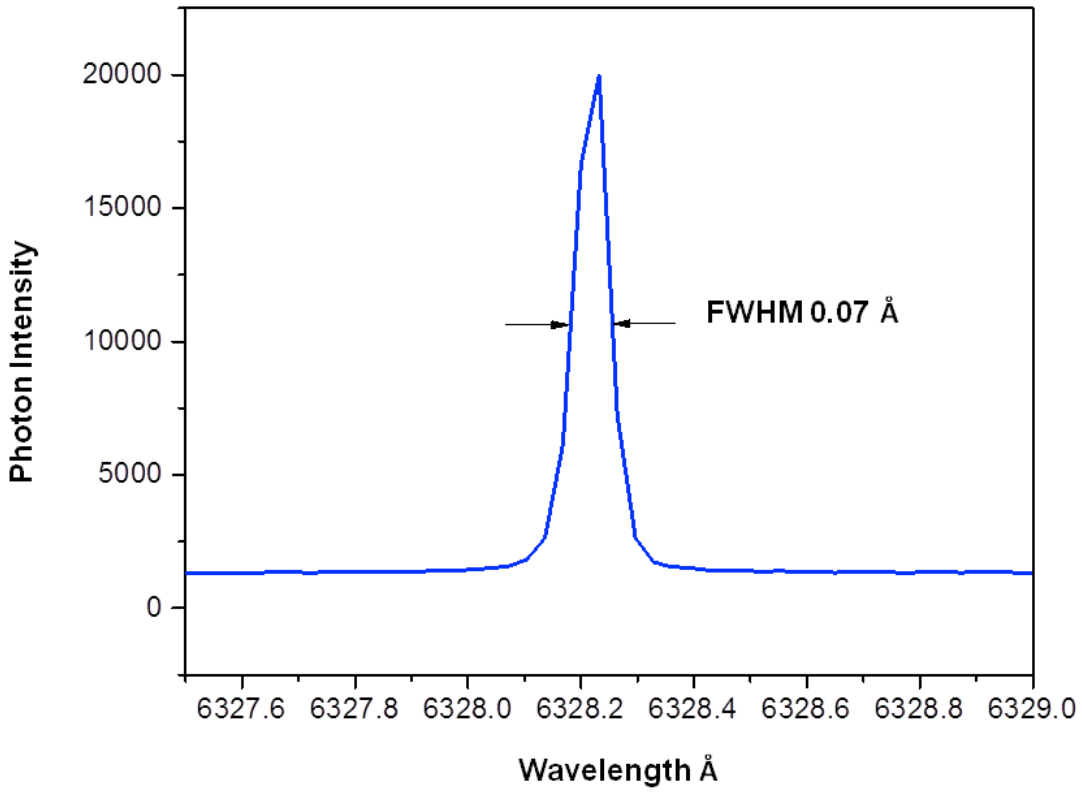
20000
15000
10000
5000
0
Photon Intensity
FWHM 0.07 Å
6327.6
6327.8
6328.0
6328.2
6328.4
6328.6
6328.8
6329.0
Wavelength Å

(A)

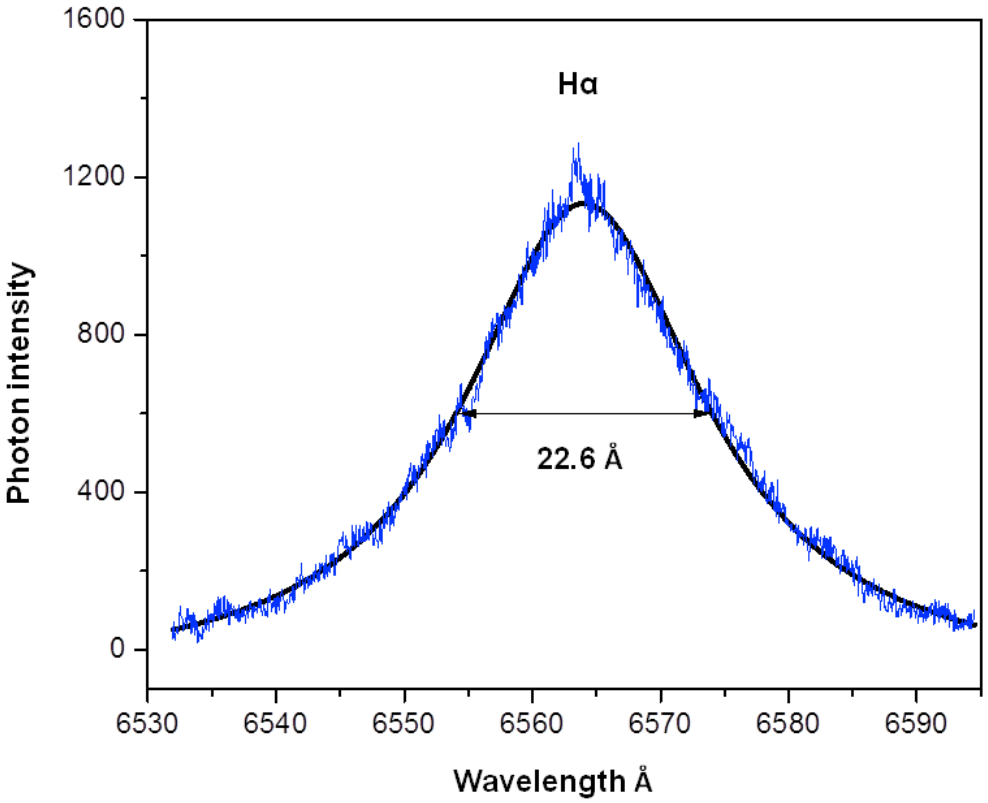

(B)

Figure 13. High resolution, visible spectra in the spectral region of the H Balmer α line measured using the Jobin Yvon Horiba 1250 M spectrometer with a 20 μm slit. (A) The full width half maximum (FWHM) of the 632.8 nm HeNe laser line was 0.07 Å that confirmed the high spectral resolution. (B) The FWHM of the Balmer α line from the emission of the ignited solid fuel 100 mg Cu + 30 mg H_2O sealed in the DSC pan was 22.6 Å corresponding to an electron density of $3.96\times10^{23}/m^3$. The line was shifted by +1.2 Å. During a phase of the event, the plasma was almost completely ionized.

4. 5 Spectroscopic measurement of the visible optical power balance

The visible energy density spectrum of the plasma following ignition of the solid fuel 80 mg Ti + 30 mg H_2O sealed in the DSC pan recorded with the Ocean Optics spectrometer is shown in Figure 14. As determined from the Stark broadening (section 4.4), during a phase of the ignition event, the plasma is essentially 100% ionized; consequently, it is a blackbody radiator [42]. The spectral profile closely matching that of the Sun (Figure 10) corresponds to the

blackbody temperature of about 5000 K. This temperature can be used to calculate the irradiance *R* or power per unit area that can be compared to the measured irradiance. In contrast, no blackbody emission was observed in the visible region when the Al pan alone was run in the absence of H_2O-based solid fuel. Only line emission was observed.

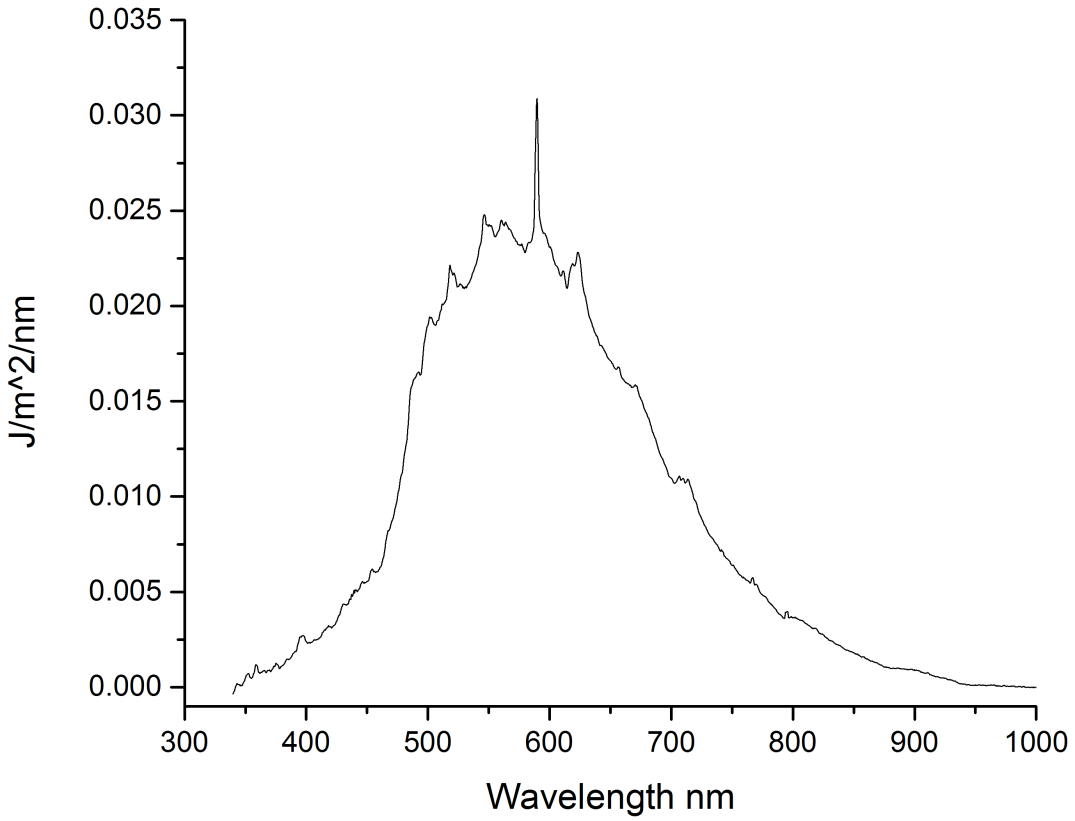

Figure 14. The optical energy density spectrum (350 nm to 1000 nm) measured with the Ocean Optics spectrometer by temporal integration of the power density spectrum taken over a time span of 5 s to collect all of the optical energy from the 0.5 ms light emission pulse of the ignited solid fuel 80 mg Ti + 30 mg H_2O sealed in a DSC pan. The energy density obtained by integrating the energy density spectrum was 5.86 J/m^2 recorded at a distance of 353.6 cm.

From Wien's displacement law [43], the wavelength λ_{max} having the greatest energy density of a blackbody at T= 5000 K is

$$\lambda_{max} = \frac{hc}{4.965kT} = 580 \text{ nm} \tag{10}$$

The Stefan-Boltzmann law [43] equates the power radiated by an object per unit area, R, to the emissivity, e, times the Stefan-Boltzmann constant, σ, times the fourth power of the temperature, T^4.

$$R = e\sigma T^4 \tag{11}$$

The emissivity $e = 1$ for an optically thick plasma comprising a blackbody [42], $\sigma = 5.67\times10^{-8}$ $Wm^{-2}K^{-4}$, and the measured blackbody temperature is 5000 K. Thus, the power radiated per unit area by the ignited solid fuel is

$$R = (1)\left(\sigma = 5.67\times10^{-8}\ \mathrm{Wm^{-2}K^{-4}}\right)\left(5000\,\mathrm{K}\right)^4 = 35\times10^{6}\ \mathrm{Wm^{-2}} \tag{12}$$

As reported in section 4.2, the measured propagation velocity of the expanding plasma is sound speed. The radius average r_{ps} of the plasma sphere of 5000 K can be calculated from the sound speed propagation velocity and the temporal evolution of the light emission duration. Using the sound speed of 343 m/s (Figure 9) and the 500 μs duration recorded with the fast photodiode (Figure 11) on solid fuel 80 mg Ti + 30 mg H_2O sealed in the DSC pan, the average radius r_{ps} of the plasma sphere is

$$r_{ps} = \frac{1/2vt^2}{t} = 8.57\ \mathrm{cm} \tag{13}$$

The optical energy density obtained by integrating the energy density spectrum measured with the Ocean Optics spectrometer was 5.86 J/m^2, recorded at a distance of 353.6 cm. Dividing the measured optical energy density by the pulse duration time of 5×10^{-4} s gives the power density at the stand-off distance of 353.6 cm. The power density at the average radius of the plasma sphere is given by multiplying by the square of the ratio of the standoff radius and the average plasma sphere radius $(353.6\ \mathrm{cm}/8.57\ \mathrm{cm})^2$. The resulting measured optical power is 21 MW/m^2 in good agreement with equation (12) considering that the optically measured power in the visible range increased by 70% with a back stream of gas flow to partially remove the optically thick metal powder dust created by the blast and further considering that some energy is outside of the wavelength region of the spectrometer.

4. 6 EUV spectra of ignited solid fuels

A wavelength calibration emission spectrum (0–45 nm) of a high voltage pulsed discharge in air (100 mTorr) with Al filters (Figure 15) showed only known oxygen and nitrogen lines and the zero order peak in the absence of a continuum.

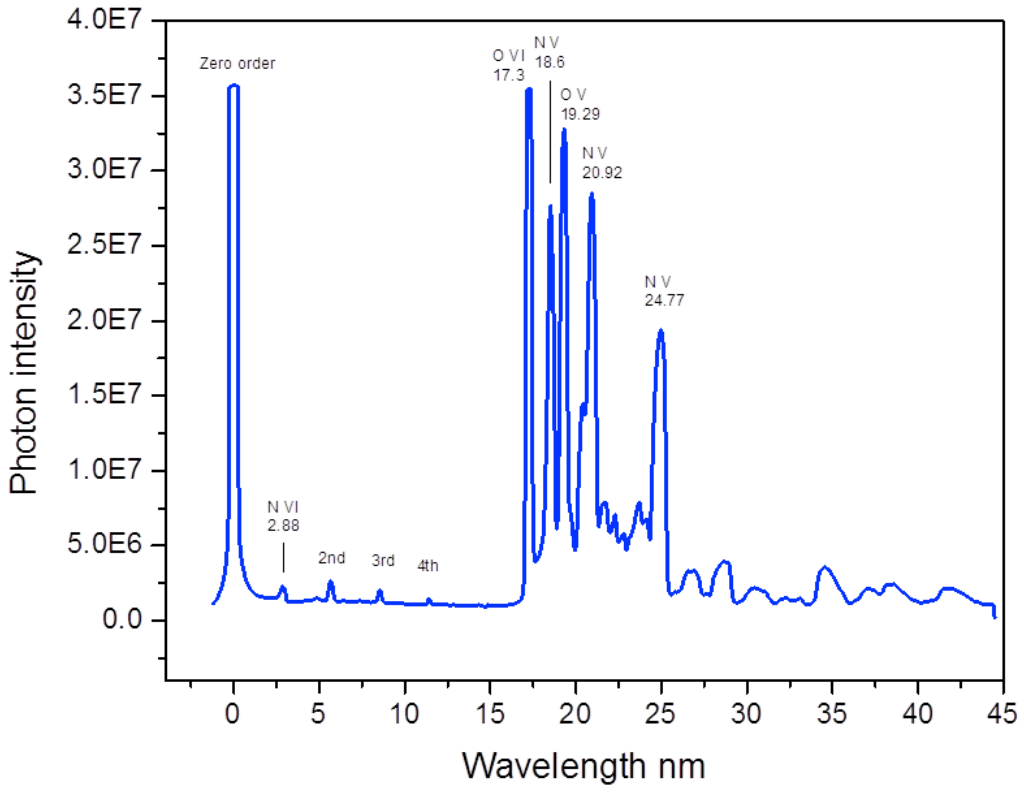

Figure 15. Calibration emission spectrum (0–45 nm) of a high voltage pulsed discharge in air (100 mTorr) with W electrodes recorded using the EUV grazing incidence spectrometer with the 600 lines/mm grating and Al filters showing that only known oxygen and nitrogen lines and the zero order peak were observed in the absence of a continuum.

Remarkably, a band of EUV emission was observed in the same region of 17 nm to 40 nm with an intense EUV zero order peak in the spectrum (Figure 16) of the NiOOH solid fuel that was ignited to a plasma by high current in the absence of a high voltage. The Al filter was confirmed to be intact following the recording of the blast spectrum. A second spectrum recorded on another ignited solid fuel sample with a quartz window of 1/4" thickness (that cuts any EUV light but passes visible light) placed in the light path showed a flat spectrum confirming that the short wavelength photon signal was not due to scattered visible light that passed the Al filters. The blast spectra showed a signal cut off below 17 nm that was due to Al filter transmittance notch (Figure 4(A)). The radiation of energy greater than 70 eV (shorter wavelength than 17 nm photons) is not possible due to field acceleration since the maximum applied voltage of the power supply was less than 15 V. As confirmation, application of high

current to a stand-alone sample of the solid fuel with the power source instrumented with fast parameter diagnostics showed the detonation occurred with a current of about 10,000 A, a voltage of about 5 V, and an input energy of less than 5 J. No EUV radiation was observed when the Al pan was run without the H_2O-based solid fuel. Moreover, no known chemical reaction can release more than a few eVs. To eliminate any possible chemical reaction as a source of plasma energy, a solid fuel comprising Ag and Cu metals and hydrated BaI_2 with no known exothermic chemistry was run.

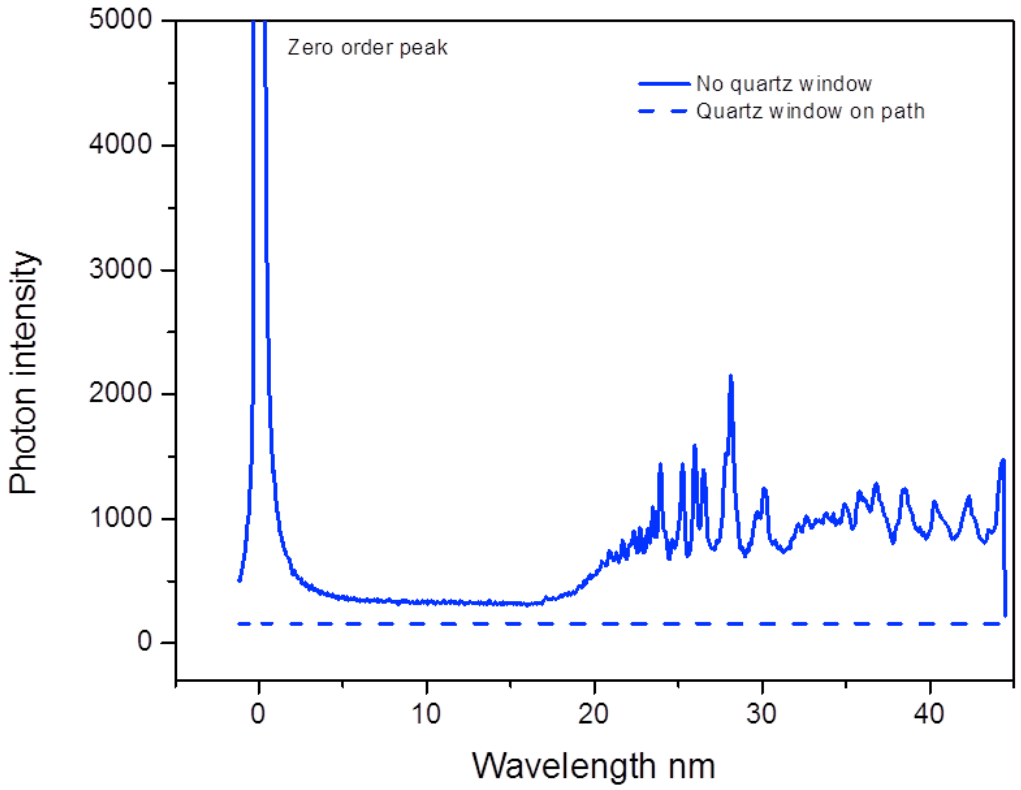

Figure 16. Emission spectra (0–45 nm) of the plasma emission of the conductive NiOOH pellet ignited with a high current source having an applied AC peak voltage of less than 15 V recorded with two Al filters alone and additionally with a quartz filter. Only EUV passes the Al filters, and the EUV light is blocked by the quartz filter. A strong EUV continuum with secondary ion emission was observed in the region 17 nm to 45 nm with a characteristic Al filter notch at 10 nm to 17 nm as shown in Figure 4(A). The EUV spectrum (0–45 nm) and intense zero order peak were completely cut by the quartz filter confirming that the solid fuel plasma emission was EUV.

The emission spectrum (0–45 nm) of the plasma emission of a 3 mm pellet of the conductive Ag (10%)-Cu/BaI_2 $2H_2O$ fuel ignited with a high current source having an applied AC peak voltage of less than 15 V recorded with two Al filters showed strong EUV continuum with secondary ion emission in the region 17 nm to 45 nm with a characteristic Al filter notch at 10 nm to 17 nm (Figure 17). The radiation band in the region of 40 nm to less than 17 nm with the shorter wavelengths cut by the Al filters matched the theoretically predicted transition of H to the hydrino state H(1/4) according to equations (5)–(9).

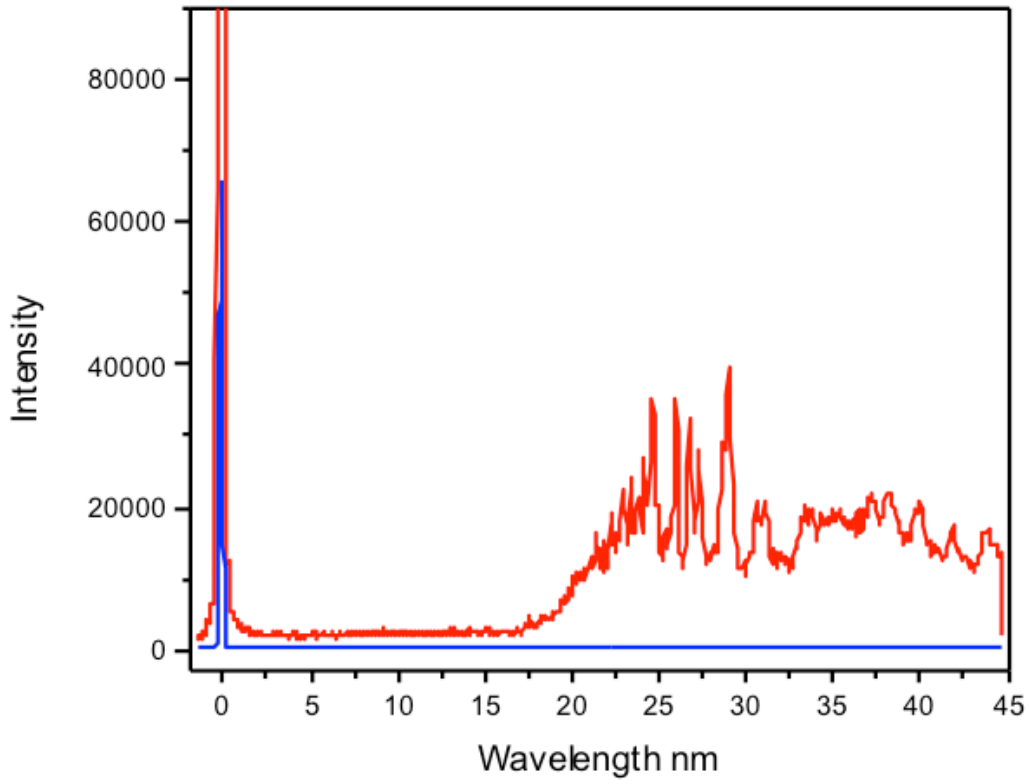

Figure 17. Emission spectrum (0–45 nm) of the plasma emission of a 3 mm pellet of the conductive Ag (10%)-Cu/BaI_2 $2H_2O$ fuel ignited with a high current source having an applied AC peak voltage of less than 15 V recorded with two Al filters with a superimposed expansion to present details. A strong EUV continuum with secondary ion emission was observed in the region 17 nm to 45 nm with a characteristic Al filter notch at 10 nm to 17 nm as shown in Figure 4(A).

To search for the 10.1 nm short wavelength cutoff of the H(1/4) transition continuum radiation while selectively blocking visible light, a 150 nm thick Zr filter (Luxel Corporation) that has a transmission window in the region of 10 nm (Figure 4(B)) was placed in the light path between the grating and CCD detector. The emission spectrum (0–45 nm) of the plasma emission of a 3 mm pellet of the conductive Ag (10%)-Cu/BaI_2 $2H_2O$ fuel ignited with the high current AC source showed strong EUV continuum having a 10.1 nm cutoff as predicted by equations (8)–(9) as shown in Figure 18. The lines observed in the high-energy EUV region (Figures 16–18) must be due to ion lines of the solid fuel material from the absorption of high-energy from a source other than the electric field. The emission lines are expected on top of the hydrino continuum radiation due to absorption of this background radiation and reemission as spectral lines. The same mechanism applies to H pinch plasma emission, and it explains the presence of highly ionized ions of nonthermal nature in the Sun and other astronomical sources as shown in section 4.9.

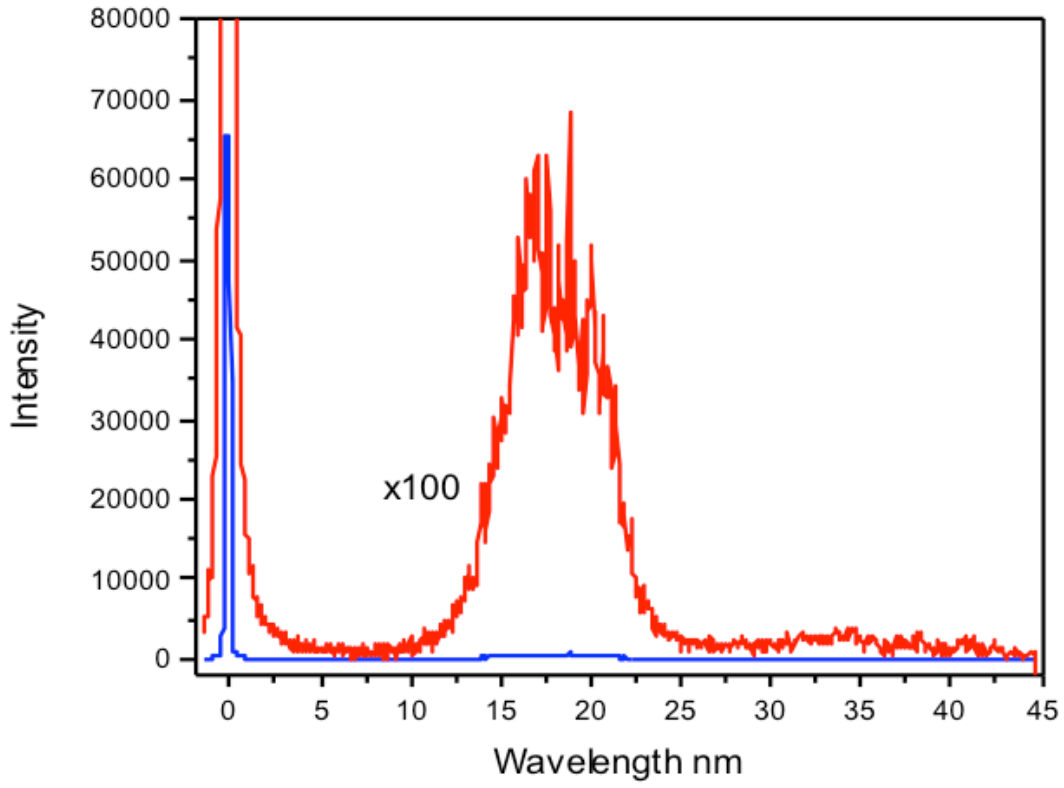

Figure 18. Emission spectrum (0–45 nm) of the plasma emission of a 3 mm pellet of the conductive Ag (10%)-Cu/BaI_2 $2H_2O$ fuel ignited with a high current source having an applied

AC peak voltage of less than 15 V recorded with a Zr filter with a superimposed expansion to present details. A strong EUV continuum with secondary ion emission was observed having a 10.1 nm cutoff as predicted by equations (8)–(9) that was transmitted by the zirconium filter as shown in Figure 4(B).

In addition to HOH, *m*H atom catalyst was tested as evidenced by the observation of EUV radiation from a solid fuel comprising a highly conductive material and a source of hydrogen such as a hydrocarbon. As in the case of H_2O-based solid fuels, paraffin wax in the DSC pan was detonated with a low voltage (<15 V), high current (10,000–30,000 A). No EUV light was observed from the Al DSC pan that was initially dehydrated by heating in vacuum or an inert atmosphere. However, the EUV spectrum (Figure 19) of wax in the DSC pan showed EUV radiation in the zero order that was significant enough to be confirmatory of *m*H serving as a catalyst to form hydrinos. As in the case of HOH produced EUV, there is no conventional explanation. The EUV intensity may be less than proportional to heat that was observed calorimetrically [7] due to the expanding plasma being optically thick. Moreover, ignition of a hydrocarbon-based solid fuel may produce some matching conditions as those that exist on the surface of the Sun and stars such as white dwarf stars, essentially liquid density of H atoms of a blackbody radiator at 5500–6000 K. So, the kinetics of hydrino formation should be appreciable with the high densities of H formed in the ignition plasma with the presence of the arc current condition. The most favorable transition based on the kinetics of multi-body reactions is H to H(1/2) that has continuum radiation with $\lambda \geq 91.2 \text{ nm}$, outside the range of the grazing incidence EUV spectrometer and Al filter. The observation of the lower intensity zero order EUV is consistent with expectations.

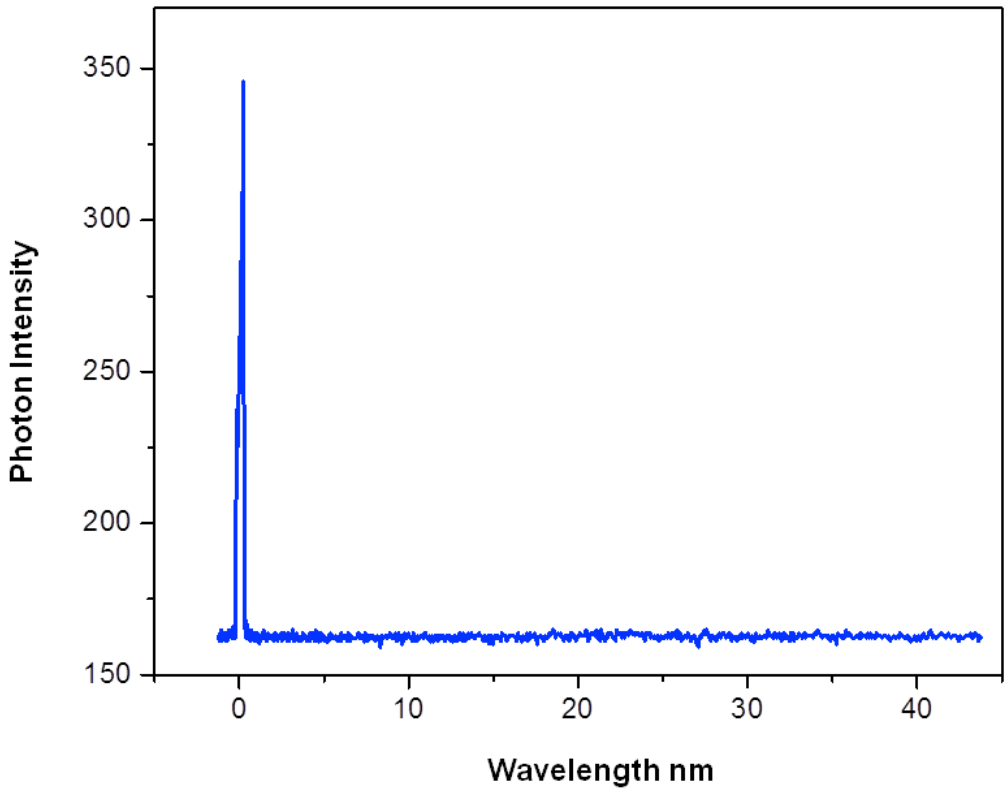

Figure 19. Emission spectra (0–45 nm) of the plasma emission of paraffin wax sealed in the conductive DSC pan ignited with a high current source having an applied AC peak voltage of less than 15 V recorded with the two Al filters alone and additionally with a quartz filter. A zero order EUV peak was observed.

4. 7 Spectroscopic measurement of the EUV optical power balance

The emission spectra (0–45 nm) of the plasma emission of a second conductive NiOOH pellet ignited with a high current source having an applied AC peak voltage of less than 15 V recorded with two Al filters alone and additionally with a quartz filter are shown in Figure 20. An extraordinarily intense zero order peak and EUV continuum was observed due to EUV photon scattering of the massive emission and large slit width of 100 μm. The EUV spectrum (0–45 nm) and zero order peak was completely cut by the quartz filter confirming that the solid fuel plasma emission was EUV. The emission comprised 2.32×10^{7} photon counts. Using a standard energy light source, the total energy of the EUV emission can be determined.

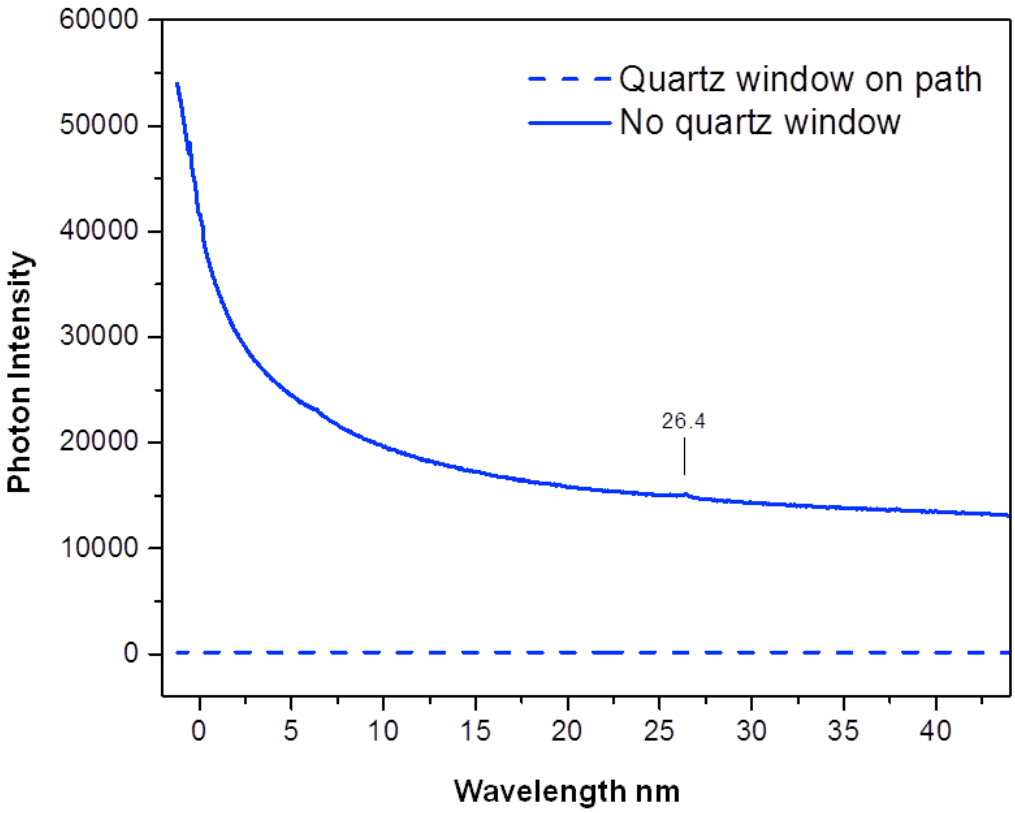

Figure 20. Emission spectra (0–45 nm) of the plasma emission of a conductive NiOOH pellet ignited with a high current source having an applied AC peak voltage of less than 15 V recorded with two Al filters alone and additionally with a quartz filter. An extraordinarily intense zero order peak and EUV continuum was observed due to EUV photon scattering of the massive emission and large slit width of 100 μm. The emission comprised 2.32×10^7 photon counts that corresponded to a total distance-and-solid-angle-corrected energy of 148 J of EUV radiation. The EUV spectrum (0–45 nm) and zero order peak were completely cut by the quartz filter confirming that the solid fuel plasma emission was EUV.

According to prior experimental pinch plasma observations [44], the total energy E_T is the sum of the joule heating energy E_j and the radiation energy E_r wherein the joule heating energy E_j is about equivalent to the radiation energy E_r:

$$E_j \approx E_r \tag{14}$$

The energy stored in the capacitors E_C having capacitance C = 104 nF and voltage V = 10,000 V is

$$E_{\mathrm{C}} = \frac{1}{2} CV^2 = (0.5)\left(104 \times 10^{-9}\right)\left(1 \times 10^{4}\right)^2 = 5.2 \text{ J} \tag{15}$$

From equation (14),

$$E_{\mathrm{r}} = \frac{5.2 \text{ J}}{2} = 2.6 \text{ J} \tag{16}$$

Based on the spectrum shown in section 4.1, the EUV radiation is more than 95% of the total radiation, which is extraordinary and characteristic of the hydrino reaction. Thus, E_{r} becomes

$$E_{\mathrm{r}} = (0.95)(2.6 \text{ J}) = 2.5 \text{ J} \tag{17}$$

This energy is discharged into the hydrogen gas in a volume of about 14 μl such the emission can be treated as a point source. Next, the correction for distance and solid angle is calculated. The distance from plasma to spectrometer slits was 750 mm. Thus, using equation (17), the incident EUV energy density E_{i} of the H_2 pinch plasma at the slits was

$$E_{\mathrm{i}} = \frac{E_{\mathrm{r}}}{4\pi(750 \text{ mm})^2} = \frac{2.5 \text{ J}}{4\pi(750 \text{ mm})^2} = 3.54 \times 10^{-7} \text{ J/mm}^2 \tag{18}$$

Using the slit dimensions, the photon energy E_s passing through the 50 um slits was

$$E_s = (2 \text{ mm})(50 \; X \; 10^{-3} \text{ mm})(3.54 \; X \; 10^{-7} \; J / \text{mm}^2) = 3.54 \; X \; 10^{-8} \text{ J} \tag{19}$$

Correcting for the grating efficiency for EUV of 15%, the CCD quantum efficiency (QE) for EUV of 90%, the Al filter transmission rate (0.15 um Al foil) of 80%, and the Al filter transmission rate (0.8 um Al foil) of 15% gives a calculated detection energy E_{cal} of

$$E_{cal} = (0.15)(0.90)(0.80)(0.15)(3.54 \; X \; 10^{-8} \text{ J}) = 5.73 \; X \; 10^{-10} \text{ J} \tag{20}$$

The total EUV photon counts of the calibration H_2 pinch plasma spectrum was 391759. Using the average photon wavelength of 40 nm wherein the Al filter has a band pass from 17 to 80 nm, the corresponding measured or observed energy E_{obs} was

$$E_{obs} = (391759 \; photons)(4.97 \; X \; 10^{-18} \text{ J} / \; photon) = 1.95 \; X \; 10^{-12} \text{ J} \tag{21}$$

The ratio of the calculated (E_{cal}) and observed energy (E_{obs}) given by equations (20) and (21) calibration factor C_0 is

$$C_0 = \frac{E_{cal}}{E_{obs}} = \frac{5.73 \; X \; 10^{-10} \text{ J}}{1.95 \; X \; 10^{-12} \text{ J}} = 294 \tag{22}$$

This factor accounts for other inefficiencies in the detection.

The total EUV photon counts of the NiOOH ignition plasma spectrum (Figure 20) was 23170428. Using equation (21) gives an observed energy E_{obs} of

$$E_{obs} = (23170428 \; photons)(4.97 \; X \; 10^{-18} \text{ J} / \; photon) = 1.15 \; X \; 10^{-10} \text{ J} \tag{23}$$

Correcting E_{obs} of equation (23) by C_0 (equation (22)), and the efficiencies of the grating, CCD QE, and two Al foils (equation (20)), the photon energy E_s passing through the slit was

$$E_s = C_0 \frac{E_{obs}}{(0.15)(0.90)(0.80)(0.15)} = (294)\frac{1.15\ X\ 10^{-10}\ \text{J}}{(0.15)(0.90)(0.80)(0.15)} \quad (24)$$
$$= 2.09\ X\ 10^{-6}\ \text{J}$$

Using equation (24) and (19), the EUV incident energy density E_i of the ignition plasma at the 100 um slits was

$$E_i = \frac{E_s}{(2\ \text{mm})(100\ X\ 10^{-3}\ \text{mm})} = \frac{2.09\ X\ 10^{-6}\ \text{J}}{(2\ \text{mm})(100\ X\ 10^{-3}\ \text{mm})} = 1.05\ X\ 10^{-5}\ J/\text{mm}^2 \quad (25)$$

In the case that the average radius of the plasma was 85.7 mm (equation (13)), the blast energy density at the radius of the emitting plasma $E_{r(ps)}$ was

$$E_{r(ps)} = 1.05\ X\ 10^{-5}\ \text{J/mm}^2 \left(\frac{750\ \text{mm}}{85.7\ \text{mm}}\right)^2 = 8.04\ X\ 10^{-4}\ \text{J/mm}^2 \quad (26)$$

Equation (14) takes into consideration that about 1/2 of the energy input to a plasma such as the H_2 pinch plasma is dissipated in joule heating from plasma resistive power (I^2R). In the case of the ignition plasma there is no such resistive heating to diminish the radiative energy component of the total energy. However, there is loss of the radiative energy by absorption. The detonation plasma initiated at the optically thick condition of atmospheric pressure and expanded into vacuum in the chamber of the EUV spectroscopy setup to become optically thin. However, the EUV radiation was down-converted into visible radiation until the plasma became at least partially transparent to EUV. The total energy E_T is given by integration of $E_{r(ps)}$ (equation (26)) over the solid angle at the radius r_{ps} given by equation (13). Using equation (18) with equation (14), that reasonably corrects for counting only the transmitted EUV radiation energy, gives a total EUV energy E_T of

$$E_T = (2)\left(4\pi r_{ps}^2 E_{r(ps)}\right) = 8\pi(85.7\ \text{mm})^2\ 8.04\ X\ 10^{-4}\ \text{J/mm}^2 = 148\ \text{J} \quad (27)$$

As discussed in section 4.6, the electric field ionization of charged particles and subsequent recombination emission in the EUV energy region is not possible due to the low applied field and the high collisional nature of the dense conditions immediately following the blast. Conventional reactions cannot produce light in this high-energy region. Moreover, the decomposition of 2NiOOH to $Ni_2O_3 + H_2O$ is endothermic [45]; so, no energy is even expected. The massive EUV emission is the source of ionization to form essentially fully ionized plasma (section 4.2) and highly ionized ions as shown in Figures 16–18 that is extraordinary given the atmospheric pressure condition. Highly ionized ions are also formed by absorption of the continuum radiation background shown in Figures 5(A)–(D) and Figure 6 wherein the plasma is optically thin with an otherwise insufficiently low electron temperature of <10 eV.

The emission spectra (0–45 nm) of the plasma emission of 5 mg energetic material NH_4NO_3 sealed in the conductive Al DSC pan ignited with a high current source having an applied AC peak voltage of less than 15 V recorded with two Al filters alone and additionally with a quartz filter are shown in Figure 21. An extraordinarily intense zero order peak was observed as shown by comparison with H_2 pinch discharge emission (lower trace) recorded using the methods of section 3.1. The EUV spectrum (0–45 nm) and zero order peak was completely cut by the quartz filter confirming that the solid fuel plasma emission was EUV. The emission comprised 9.82×10^6 photon counts. Using the calibration factor C_0 (equation (22)) and efficiency and dimensional corrections, the total energy of the EUV emission can be determined.

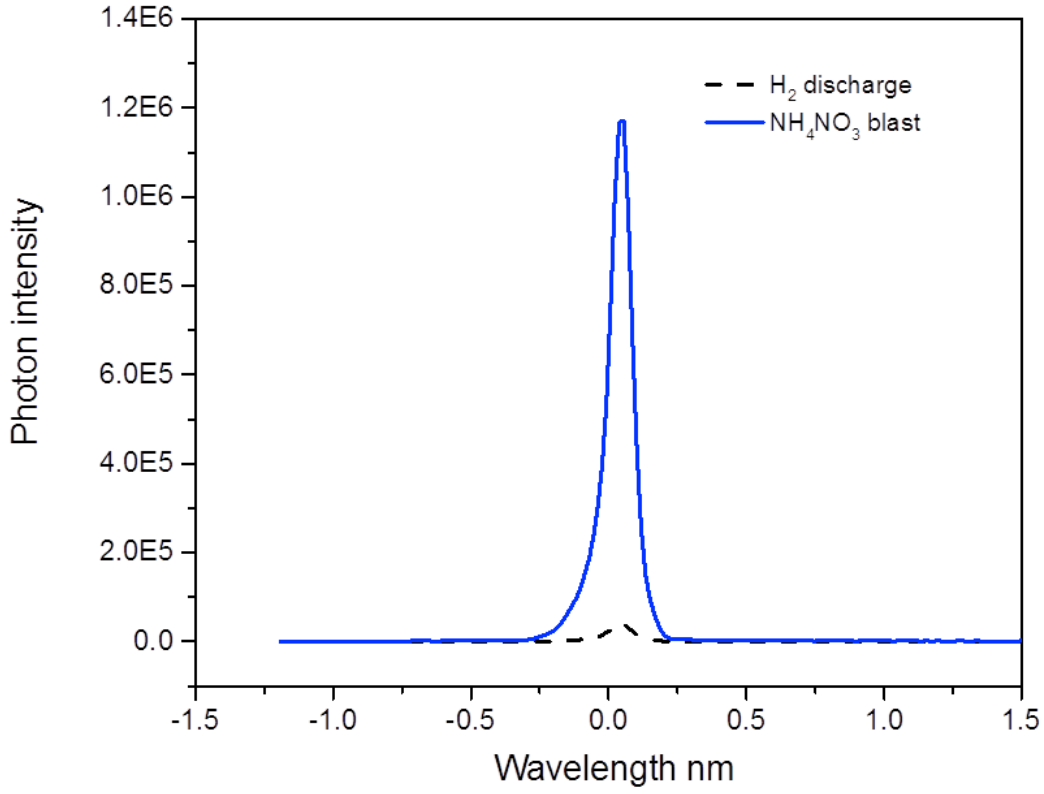

Figure 21. Emission spectra (0–45 nm) of the plasma emission of 5 mg energetic material NH_4NO_3 sealed in the conductive Al DSC pan ignited with a high current source having an applied AC peak voltage of less than 15 V recorded with two Al filters. An extraordinarily intense zero order peak was observed as shown by the comparison with H_2 pinch discharge emission (lower trace) recorded using the methods of section 3.1. The emission corresponded to a total distance-and-solid-angle-corrected energy of 125 J of EUV radiation.

The total EUV photon counts of the NH_4NO_3 ignition plasma spectrum (Figure 21) is 9818041. Using equation (21) gives an observed energy E_{obs} of

$$E_{obs} = \left(9818041\ photons\right)\left(4.97\ X\ 10^{-18}\ \text{J}\ /\ photon\right) = 4.88\ X\ 10^{-11}\ \text{J} \tag{28}$$

Correcting E_{obs} of equation (28) by C_0 (equation (22)), and the efficiencies of the grating, CCD QE, and two Al foils (equation (20)), the photon energy E_s passing through the slit was

$$E_s = C_0 \frac{E_{obs}}{\left(0.15\right)\left(0.90\right)\left(0.80\right)\left(0.15\right)} = \left(294\right)\frac{4.88\ X\ 10^{-11}\ \text{J}}{\left(0.15\right)\left(0.90\right)\left(0.80\right)\left(0.15\right)} \tag{29}$$
$$= 8.86\ X\ 10^{-7}\ \text{J}$$

Using equations (29) and (19), the EUV incident density E_i of the ignition plasma at the 50 um slits was

$$E_i = \frac{E_s}{\left(2\ \text{mm}\right)\left(50\ X\ 10^{-3}\ \text{mm}\right)} = \frac{8.86\ X\ 10^{-7}\ \text{J}}{\left(2\ \text{mm}\right)\left(50\ X\ 10^{-3}\ \text{mm}\right)} = 8.86\ X\ 10^{-6}\ \text{J/mm}^2 \tag{30}$$

In the case that the average radius of the plasma was 85.7 mm (equation (13)), the blast energy density at the radius of the emitting plasma $E_{r(ps)}$ was

$$E_{r(ps)} = 8.86\ X\ 10^{-6}\ \text{J/mm}^2\left(\frac{750\ \text{mm}}{85.7\ \text{mm}}\right)^2 = 6.79\ X\ 10^{-4}\ \text{J/mm}^2 \tag{31}$$

The total energy E_T is given by integration of $E_{r(ps)}$ (equation (31)) over the solid angle at the radius r_{ps} given by equation (13). Using equation (18) with equation (14), that reasonably corrects for counting only the transmitted EUV radiation energy, gives a total EUV energy E_T of

$$E_T = \left(2\right)\left(4\pi r_{ps}^2 E_{r(ps)}\right) = 8\pi\left(85.7\ \text{mm}\right)^2 6.79\ X\ 10^{-4}\ \text{J/mm}^2 = 125\ \text{J} \tag{32}$$

The solid fuel NH_4NO_3 is a well-known energetic material that does release energy upon thermal decomposition. The decomposition reaction of NH_4NO_3 to N_2O and H_2O calculated from the heats of formation [46–48] is exothermic by $\Delta H = -124.4$ kJ/mole NH_4NO_3:

$$NH_4NO_3 \rightarrow N_2O + 2H_2O \tag{33}$$

At elevated temperature, further decomposition occurs. The decomposition reaction energy of NH_4NO_3 to N_2, O_2, and H_2O calculated from the heats of formation [46–48] is exothermic by $\Delta H = -206$ kJ/mole NH_4NO_3:

$$NH_4NO_3 \rightarrow N_2 + 1/2O_2 + 2H_2O \tag{34}$$

For 5 mg NH_4NO_3, the theoretical energy release is 12.8 J (equation (34)). Assuming slow kinetics for the oxidation of Al metal pan [49], the experimental calorimetrically measured energy balance was reported previously [7] to be 442.7 J, 34.6 times the most exothermic conventional chemistry reaction given by equation (10). The high excessive energy balance was

confirmed by replacing the conductive Al matrix with non-reactive Ag [7]. The soft X-ray emission energy of 125 J (equation (32)) is 10 times the theoretical energy considering this component alone. The additional energy is attributed to the formation of hydrino. The observation of massive soft X-ray confirms hydrogen has lower energy levels. The hydrino reaction produces 200 times the energy of the conventional chemistry of high explosives that have CHNO structures favorable for forming HOH and H (equations (5)–(8)). The emission of soft X-rays from energetic material NH_4NO_3 is very strong evidence that the mechanism of shock wave production in high explosives comprising a source of H and HOH such as those having the elemental composition CHNO is based on the extraordinary energy released by the formation of $H_2(1/4)$. Indeed, $H_2(1/4)$ was observed spectroscopically as the product of the gun powder reaction and the reaction of NH_4NO_3 as reported previously [30], and EUV continuum radiation (1500 counts of zero order radiation) was observed from gun powder in the present studies. The extraordinary energy and hydrino product identification have ramifications for an approach to exploiting the hydrino mechanism of the shock wave of energetic materials to enhance this property. As given in section 4.2, all of the H_2O-based solid fuels ignited and produced a shock wave behaving as energetic materials with the exception that essentially all the power was in the form of visible radiation rather than pressure-volume. The powers and power densities were extraordinary [7].

4.8 LED power balance of SF-CIHT cell having photovoltaic conversion

The detonations of solid fuel 80 mg Ti + 30 mg H_2O produced brilliant flashes of light with white color consistent with the measured blackbody temperature of over 5000 K (section 4.2). The visible light was appropriate for solar photovoltaic conversion. The series of sequential detonations of the Ti + H_2O pellets at 1 Hz maintained the LED array at essentially continuous operation at full light output. Consider the balance of the energy released by the solid-fuel-pellet detonations and the energy collected by the three solar panels. On average per fuel pellet, the LEDs output about 60 W for about 1 s even though the blast even was much shorter, 500 μs (section 4.2). The polycrystalline photovoltaic material had a response time and maximum power that was not well suited for a megawatt short burst. But, due to some capacitance, the solar cells served as a load leveler of the about 60 J energy over the 1 s time interval per pellet detonation. The reflection of the light at the Lexan was determined to be about 40% with a corresponding transmission of 60%, and the polycrystalline cells were rated to have a maximal efficiency of 12% at converting 5800 K light into electricity. Thus, the effective efficiency was about 7.2%. Not including the light lost from the backside, top, and bottom of the plasma, correcting the 60 J for the 7.2% efficiency corresponds to 833 J. This energy matches the measured calorimetric energy balance reported previously [7] as well as the optical power balance given in section 4.5

wherein corresponding optical power incident on the solar panel over the 500 μs ignition event was 1.67 MW (833 J/500 μs). The typical energy to cause detonation was about 60 J for these DSC pellets that required melting followed by detonation. The corresponding energy gain was about 14×. Twenty-five year warranty, triple junction concentrator photovoltaics (PV) at high power irradiation have achieved over 40% conversion efficiency at over 1 MW/m^2, and new generation PV cells are being developed with 10 times this intensity capability. Commercial viability is demonstrated by these results.

4. 9 Astrophysical data supporting the *m*H catalyst mechanism

Our EUV continuum results offer resolution to many otherwise inexplicable celestial observations with (a) the energy and radiation from the hydrino transitions being the source of extraordinary temperatures and power regarding the solar corona problem, the cause of sunspots and other solar activity, and why the Sun emits X-rays [3], (b) the hydrino-transition radiation being the radiation source heating the WHIM and behind the observation that diffuse Hα emission is ubiquitous throughout the Galaxy requiring widespread sources of flux shortward of 912 Å, and (c) the identity of dark matter being hydrinos.

Stars also comprise plasmas of hydrogen with surfaces comprised of essentially dense atomic hydrogen permissive of multi-body H interactions to propagate transition of H to H(1/(*m* +1)) wherein *m*H serves as the catalyst. Such transitions are predicted to emit EUV continuum radiation according to equations (1)–(4) and (9). The emission from white dwarfs arising from an extremely high concentration of hydrogen is modeled as an optically thick blackbody of ~50,000 K gas comprised of predominantly hydrogen and helium. A modeled composite spectrum of the full spectral range from 10 nm to >91.2 nm with an abundance He/H=10^{-5} from Barstow and Holberg [50] is shown in Figure 1.2. Albeit, while white dwarf spectra can be curve fitted using stratification and adjustable He and H column densities and ionization fractions to remove some inconsistencies between optical and EUV spectra [51] and independent measurements of the latter, matching the spectrum at the short-wavelengths is problematic. Alternatively, combining the emission shown in Figures 5(A)–(D) with the 91.2 nm continuum observed previously [52] gives a spectrum with continua having edges at 10.1 nm, 22.8 nm, and 91.2 nm, a match to the white dwarf spectrum. However, the proposed nature of the plasmas and the mechanisms are very different. The emission in our studies is assigned to hydrino transitions in cold-gas, optically-thin plasmas absent any helium. White-dwarf and celestial models may need revision and benefit from our discovery of high-energy H continua emission.

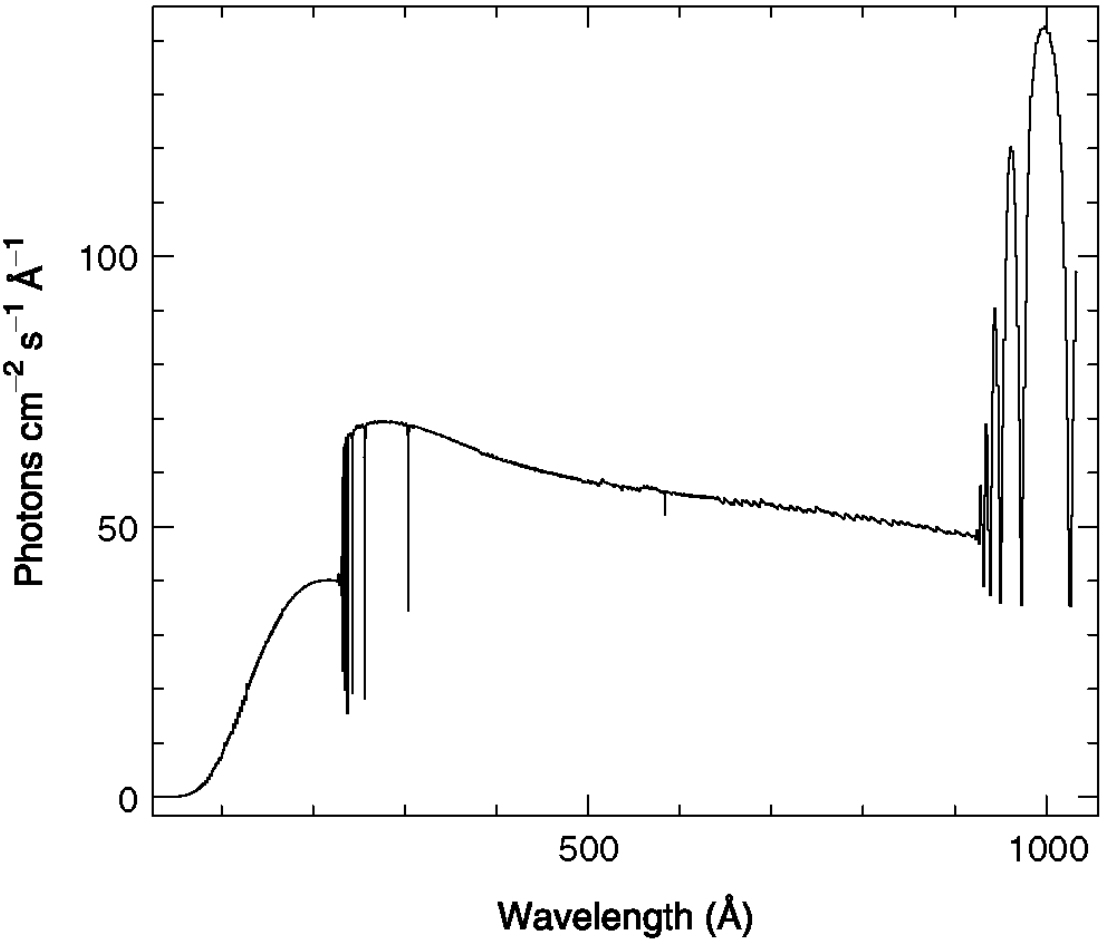

Figure 22. An exemplary model of the EUV continuum spectrum of the photosphere of a white dwarf using a temperature of 50,000 K and a number abundance of He/H = 10^{-5} showing the He II and H I Lyman absorption series of lines at 22.8 nm (228 Å) and 91.2 nm (912 Å), respectively. Reproduced by permission of Cambridge University Press [50].

For example, there is no existing physical model that can couple the temperature and density conditions in different discrete regions of the outer atmosphere (chromosphere, transition region, and corona) of coronal/chromospheric sources [51]. Seemingly in defiance of the second law of thermodynamics, the corona is typically modeled to be three orders of magnitude hotter than the surface, the source of coronal heating. Reconciliation is offered by the mechanism of line absorption and re-emission of the $m^2 \cdot 13.6$ eV (equation (9)) continuum radiation. The 91.2 nm continuum to longer wavelengths is expected to be prominent (less attenuated than the 10.1 nm and 22.8 nm bands) and is observed in the solar extreme ultraviolet spectrum as shown in Figure 23 [53] despite attenuation by the coronal gas. High-energy-photon excitation is more plausible than a thermal mechanism with T~10^6 given the 5800 K surface temperature and the

observation of the CO absorption band at 4.7 μm in the solar atmosphere wherein CO cannot exist above 4000 K [54]. Considering the 10.1 nm band as a source, the upper limit of coronal temperature based on excitation of about 10^6 K is an energy match. In addition to the temperature, another extraordinary observation is that although the total average energy output of the outer layers of the Sun is $\cong 0.01\ \%$ of the photospheric radiation, local transient events can produce an energy flux that exceeds the photospheric flux [55]. The energy source of the latter may be magnetic in nature, but the identity of the highly ionizing coronal source is not established. Nor, has the total energy balance of the Sun been reconciled. The possibility of a revolutionary discovery of a new source of energy in the Sun based on a prior undiscovered process is an open question [56]. That *m*H catalyzed hydrino transitions occur in stars and the Sun [57] as evident by corresponding continua in its spectrum resolves the solar corona problem, the cause of sunspots and other solar activity, and why the Sun emits X-rays [3].

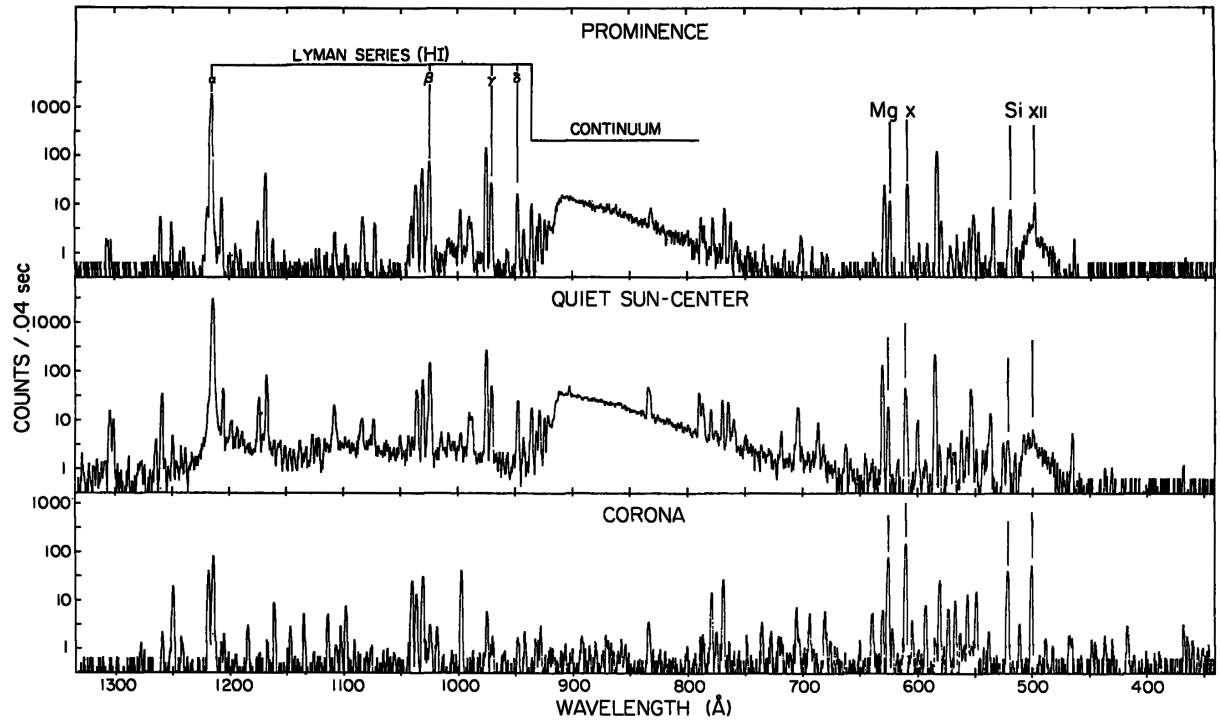

Figure 23. Skylab (Harvard College Observatory spectrometer) average extreme ultraviolet spectra of the Sun [53] recorded on a prominence (Top), quiet Sun-center (Middle), and corona above the solar limb (Bottom). In the quiet Sun-center spectrum, the 91.2 nm continuum to longer wavelengths is expected to be prominent and is observed despite attenuation by the coronal gas. The continuum was greatly reduced in the prominence and the corona wherein the H concentration was much reduced and absent, respectively. The emission from chromospheric lines and the continuum was also severely attenuated in the corona. The strongest lines in the

coronal spectrum and to a lesser extent the prominence are multiply ionized ions such as the doublets of Ne VIII, Mg X, or Si XII that could be due to absorption of high energy continuum radiation rather than thermal excitation. From Reeves et al. [58].

Our EUV continuum results have further implications for the resolution of the identity of dark matter and the identity of the radiation source behind the observation that diffuse Hα emission is ubiquitous throughout the Galaxy and widespread sources of flux shortward of 912 Å are required [59]. The identity of dark matter has been a cosmological mystery. It is anticipated that the emission spectrum of the extreme ultraviolet background of interstellar matter possesses the spectral signature of dark matter. Labov and Bowyer designed a grazing incidence spectrometer to measure and record the diffuse extreme ultraviolet background [59]. The instrument was carried aboard a sounding rocket, and data were obtained between 80 Å and 650 Å (data points approximately every 1.5 Å). Several lines including an intense 635 Å emission associated with dark matter were observed [59] which has considerable astrophysical importance as indicated by the authors:

"Regardless of the origin, the 635 Å emission observed could be a major source of ionization. Reynolds (1983, 1984, 1985) has shown that diffuse Hα emission is ubiquitous throughout the Galaxy, and widespread sources of flux shortward of 912 Å are required. Pulsar dispersion measures (Reynolds 1989) indicate a high scale height for the associated ionized material. Since the path length for radiation shortward of 912 Å is low, this implies that the ionizing source must also have a large scale height and be widespread. Transient heating appears unlikely, and the steady state ionization rate is more than can be provided by cosmic rays, the soft X-ray background, B stars, or hot white dwarfs (Reynolds 1986; Brushweiler & Cheng 1988). Sciama (1990) and Salucci & Sciama (1990) have argued that a variety of observations can be explained by the presence of dark matter in the galaxy which decays with the emission of radiation below 912 Å.

The flux of 635 Å radiation required to produce hydrogen ionization is given by $F = \zeta_{\mathrm{H}} / \sigma_{\lambda} = 4.3 \times 10^{4} \zeta_{-13}$ photons $\mathrm{cm}^{-2}\mathrm{s}^{-1}$, where ζ_{-13} is the ionizing rate in units of $10^{-13}\mathrm{s}^{-1}$ per H atom. Reynolds (1986) estimates that in the immediate vicinity of the Sun, a steady state ionizing rate of ζ_{-13} between 0.4 and 3.0 is required. To produce this range of ionization, the 635 Å intensity we observe would have to be distributed over 7%–54% of the sky."

The 63.5 ± 0.47 nm line [59] matches a hydrino transition predicted for H undergoing catalysis with H(m=1) as the catalyst giving rise to a concerted energy exchange of the total energy of

40.8 eV with the excitation of the He $1s^2$ to $1s^1 2p^1$ transition. The predicted 63.3 nm emission associated with dark matter was observed with the addition of hydrogen to helium microwave plasma as shown previously [3, 29]. An alternative assignment suggested by Labov and Bowyer [59] is the 63.0 nm line of O V requiring a large-scale non-thermal source of ionization. Continuum radiation from transitions to low-level hydrino states can provide this radiation. Indeed, the observation of the 63.3 nm line is also associated with the presence of an interstellar X-ray background.

The first soft X-ray background was detected and reported [60] about 25 years ago. Quite naturally, it was assumed that these soft X-ray emissions were from ionized atoms within hot gases. Labov and Bowyer also interpreted the data as emissions from hot gases. However, the authors left the door open for some other interpretation with the following statement from their introduction:

> "It is now generally believed that this diffuse soft X-ray background is produced by a high-temperature component of the interstellar medium. However, evidence of the thermal nature of this emission is indirect in that it is based not on observations of line emission, but on indirect evidence that no plausible non-thermal mechanism has been suggested which does not conflict with some component of the observational evidence."

The authors also state "if this interpretation is correct, gas at several temperatures is present." Specifically, emissions were attributed to gases in three ranges: $5.5 < \log T < 5.7$; $\log T = 6$; $6.6 < \log T < 6.8$. Observations in the ultraviolet with HST and FUSE [61] and also XMM-Newton [62] confirm these extraordinary temperatures of diffuse intergalactic medium (IGM) and reveal that a large component of the baryonic matter of the universe is in the form of WHIM (warm-hot ionized media) [61, 62]. The mysteries of the identity of dark matter, the observed dark interstellar medium spectrum, the source of the diffuse X-ray background, and the source of ionization of the IGM [61, 62] are resolved by the formation of hydrinos that emit EUV and X-ray continua depending on the state transition and conditions; the continua create highly ionized ions that emit ion radiation of non-thermal origin; the hydrino transition H to H(1/2) results in a 63.3 nm line [3, 29], and He^+ acting as a catalyst of 54.4 eV ($2 \cdot 27.2$ eV) pumps the intensity of helium ion lines such as the 30.4 nm line [3, 4] consistent with observations [59]. In the interstellar medium there is no required third body to collisionally take away the bond energy for the alternative process of 2H to H_2.

As shown in the Disproportionation of Energy States section of reference [1], the products of the catalysis reactions have binding energies of $m \cdot 27.2$ eV, such that they may

further serve as catalysts. Thus, further catalytic transitions may occur: $n=\frac{1}{3}\rightarrow\frac{1}{4}$, $\frac{1}{4}\rightarrow\frac{1}{5}$, and so on. Thus, lower-energy hydrogen atoms, *hydrinos*, can act as catalysts by resonantly and nonradiatively accepting energy of $m\cdot 27.2$ eV from another H or hydrino atom. Such disproportionation reactions of hydrinos are predicted to given rise to features in the X-ray region. As shown by equation (8) the reaction product of HOH catalyst is $\mathrm{H}\left[\frac{a_{\mathrm{H}}}{4}\right]$. A likely transition reaction in hydrogen clouds containing H_2O gas is the transition of a H atom to $\mathrm{H}\left[\frac{a_{\mathrm{H}}}{17}\right]$ wherein $\mathrm{H}\left[\frac{a_{\mathrm{H}}}{4}\right]$ serves as a catalyst to give a broad peak having a short wavelength cutoff at $E=3481.6$ eV; 0.35625 nm [1]. A broad X-ray peak with a 3.48 keV cutoff was recently observed in the Perseus Cluster by NASA's Chandra X-ray Observatory and by the XMM-Newton [63, 64] that has no match to any known atomic transition. The 3.48 keV feature assigned to dark matter of unknown identity by BulBul et al. [63] matches the $\mathrm{H}\left[\frac{a_{\mathrm{H}}}{4}\right]+\mathrm{H}\left[\frac{a_{\mathrm{H}}}{1}\right]\rightarrow\mathrm{H}\left[\frac{a_{\mathrm{H}}}{17}\right]$ transition and further confirms hydrinos as the identity of dark matter.

Evidence for EUV emission from hydrino transitions also comes from interstellar medium (ISM) since it provides a source of the diffuse ubiquitous EUV cosmic background. Specifically, the 10.1 nm continuum matches the observed intense 11.0–16.0 nm band [50, 65]. Furthermore, it provides a mechanism for the high ionization of helium of the ISM and the excess EUV radiation from galaxy clusters that cannot be explained thermally [66]. Moreover, recent data reveals that X-rays from distant active galactic nuclei sources are absorbed selectively by oxygen ions in the vicinity of the galaxy [67]. The temperature of the absorbing halo is between 1 million and 2.5 million Kelvin, or a few hundred times hotter than the surface of the Sun. The corresponding energy range is 86 eV to 215 eV which is in the realm of the energy released for the transition of H to H(1/4). Additional astrophysical evidence such as the observation that a large component of the baryonic matter of the universe is in the form of WHIM (warm-hot ionized media) in the absence of a conventional ionizing energy source and the match of hydrinos to the identity of dark matter was presented previously [3]. The latter case is further supported by observations of signature electron-positron annihilation energy.

Dark matter comprises a majority of the mass of the universe as well as intra-galactic mass [68, 69]. It would be anticipated to concentrate at the center of the Milky Way galaxy due to the high gravity from the presence of a super massive blackhole at the center that emits gamma rays as matter falls into it. Pair production occurs when gamma rays of sufficient energy collide with baryonic matter. Since hydrinos are each a state of hydrogen having a proton

nucleus, high-energy gamma rays impinging on dark matter will result in pair production. The corresponding observed characteristic signature being the emission of the 511 keV annihilation energy of pair production identifies dark matter as hydrino [70–72]. Another hydrino decay pathway for this radiation is given in Chp. 32 of reference [1]. Interstellar medium [73–75], gamma-ray bursts [75, 76], and solar flares [55, 75, 77] also emit 511 keV line radiation. The dominant source of positrons in gamma-ray bursts is likely pair production by photon on photons or on strong magnetic fields [75]. The solar-flare emission is likely due to production of radioactive positron emitters in accelerated charge interactions [75]; whereas, the diffuse 511 keV radiation by interstellar medium is consistent with the role of hydrino as dark matter in pair production from incident cosmic radiation [73–75].

The characteristic spectral signatures and properties of hydrino match those attributed to the dark matter of the universe. The Universe is predominantly comprised of hydrogen and a small amount of helium. These elements exist in interstellar regions of space, and they are expected to comprise the majority of interstellar matter. However, the observed constant angular velocity of many galaxies as the distance from the luminous galactic center increases can only be accounted for by the existence of nonluminous weakly interacting matter, dark matter. It was previously accepted that dark matter exists at the cold fringes of galaxies and in cold interstellar space. This has since been disproved by the observation of Bournaud et al. [68, 69] that demonstrated that galaxies are mostly comprised of dark matter, and the data persistently supports that dark matter probably accounts for the majority of the universal mass.

The best evidence yet for the existence of dark matter is its direct observation as a source of massive gravitational mass evidenced by gravitational lensing of background galaxies that does not emit or absorb light as shown in Figure 24 [78]. There has been the announcement of some unexpected astrophysical results that support the existence of hydrinos. In 1995, Mills published the GUTCP prediction [79] that the expansion of the universe was accelerating from the same equations that correctly predicted the mass of the top quark before it was measured. To the astonishment of cosmologists, this was confirmed by 2000. Mills made another prediction about the nature of dark matter based on GUTCP that may be close to being confirmed. Bournaud et al. [68, 69] suggest that dark matter is hydrogen in dense molecular form that somehow behaves differently in terms of being unobservable except by its gravitational effects. Theoretical models predict that dwarf galaxies formed from collisional debris of massive galaxies should be free of nonbaryonic dark matter. So, their gravity should tally with the stars and gas within them. By analyzing the observed gas kinematics of such recycled galaxies, Bournaud et al. [68, 69] have measured the gravitational masses of a series of dwarf galaxies lying in a ring around a massive galaxy that has recently experienced a collision. Contrary to the predictions of Cold-Dark-Matter (CDM) theories, their results demonstrate that they contain a

massive dark component amounting to about twice the visible matter. This baryonic dark matter is argued to be cold molecular hydrogen, but it is distinguished from ordinary molecular hydrogen in that it is not traced at all by traditional methods. These results match the predictions of the dark matter being molecular hydrino.

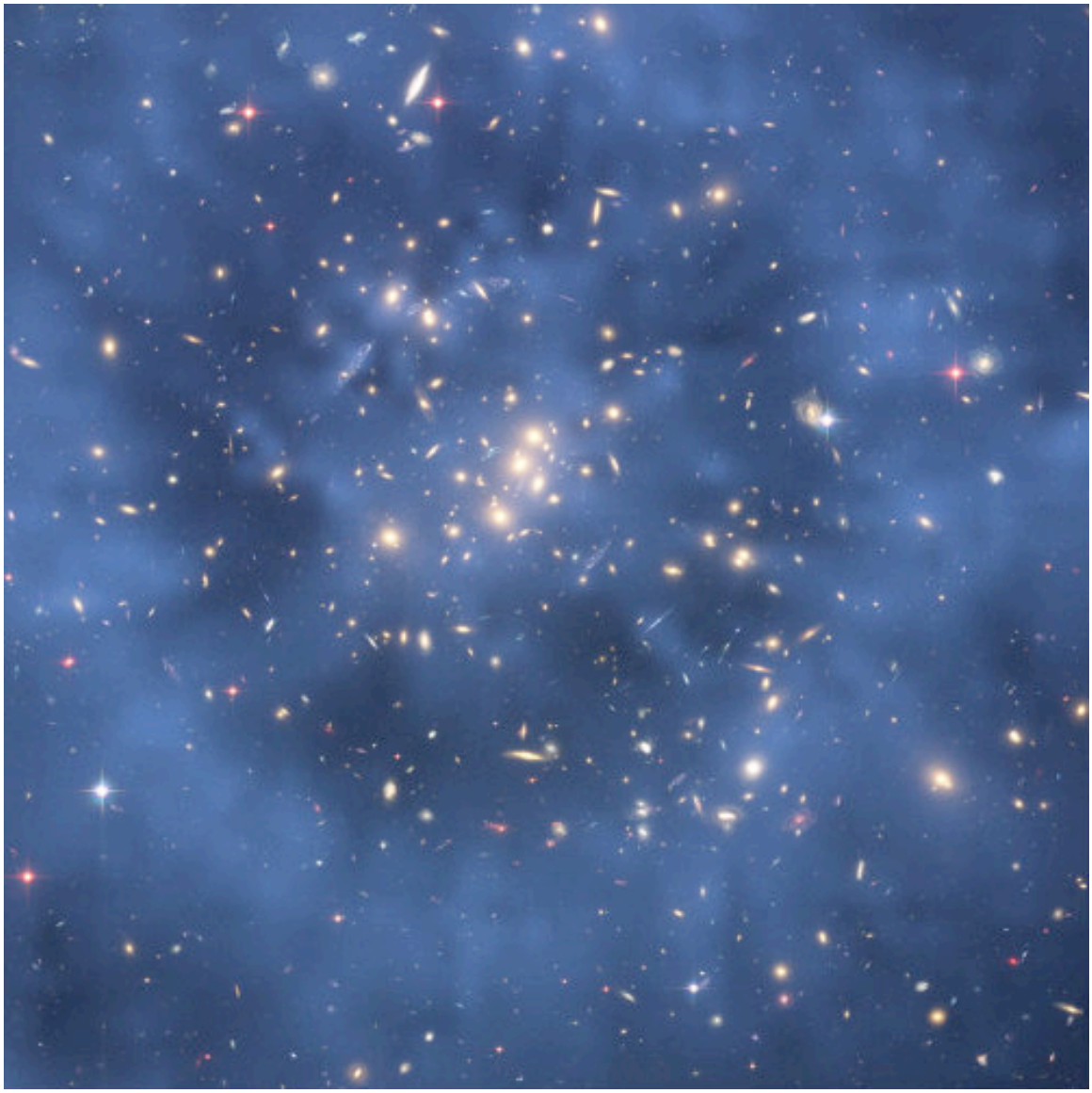

Figure 24. Dark matter ring in galaxy cluster. This Hubble Space Telescope composite image shows a ghostly "ring" of dark matter in the galaxy cluster Cl 0024+17. The ring is one of the strongest pieces of evidence to date for the existence of dark matter, a prior unknown substance that pervades the universe. Courtesy of NASA/ESA, M.J. Jee and H. Ford (Johns Hopkins University), Nov. 2004.

Additionally, astronomers Jee at al. [80] using data from NASA's Hubble Telescope have

mapped the distribution of dark matter, galaxies, and hot gas in the core of the merging galaxy cluster Abell 520 formed from a violent collision of massive galaxy clusters and have determined that the dark matter had collected in a dark core containing far fewer galaxies than would be expected if dark matter was collisionless with dark matter and galaxies anchored together. The collisional debris left behind by the galaxies departing the impact zone behaved as hydrogen did, another indication that the identity of dark matter is molecular hydrino.

Moreover, detection of alternative hypothesized identities for dark matter such as super-symmetry particles such as neutralinos has failed at the Large Hadron Collider; nor, has a single event been observed for weakly interacting massive particles or wimps at the Large Underground Xenon (LUX) experiment [81]. The HADES search for dark matter eliminated the leading candidate, "Dark Photon" or U Boson, as a possibility. This failure also undermines the Standard Model of particle physics [82].

5. Conclusion

Continuum radiation in the 10 nm to 30 nm region that matched predicted transitions of H to hydrino state H(1/4), was observed only arising from pulsed pinch hydrogen discharges with metal oxides that are thermodynamically favorable to undergo H reduction to form HOH catalyst; whereas, those that are unfavorable did not show any continuum even though the low-melting point metals tested are very favorable to forming metal ion plasmas with strong short-wavelength continua in significantly more powerful plasma sources. The plasmas showing no continuum demonstrate that the pinch source is too low energy to produce highly ionized metal continuum emission in agreement with the analysis by Bykanov [6]. Any high-energy ion emission must be due to nonthermal secondary emission from the absorbed hydrino continuum. Of the two possible catalysts, m H and HOH, the latter is more likely on the behavior with oxide coated electrodes based on the intensity profile at short wavelengths and the dependency on a thermodynamically favorable reaction of metal oxide to HOH at the anode. A similar mechanism is functional in the CIHT cell [30, 32]. In addition to characteristic continuum radiation having a short-wavelength cutoff of $m^2 \cdot 13.6$ eV; $m = 3$ for hydrino transition H to H(1/4) catalyzed by HOH, the transition also produced predicted selective extraordinary high-kinetic energy H that was observed by the corresponding broadening of the Balmer α line [5] consistent with previous observations [10].

Our laboratory experiments have celestial implications. Hydrogen continua from transitions to form hydrinos matches the emission from white dwarfs, provides a possible mechanism of linking the temperature and density conditions of the different discrete layers of the coronal/chromospheric sources, and provides a source of the diffuse ubiquitous EUV cosmic background with the 10.1 nm continuum matching the observed intense 11.0–16.0 nm band in

addition to resolving other cosmological mysteries [3, 50, 65]. *m*H catalyst was shown to be active in astronomical sources. The discovery of high-energy continuum radiation from hydrogen as it forms a more stable state has astrophysical implications such as hydrino being a candidate for the identity of dark matter and the corresponding emission being the source of high-energy celestial and stellar continuum radiation [2–6]. For example, the EUV spectra of white dwarfs matches the continua for H(1/2), H(1/3), and H(1/4), and the 10.1 nm continuum of the transition of H to H(1/4) is observed from interstellar medium. The hydrino continuum radiation matches the diffuse ubiquitous EUV and soft X-ray cosmic background [59, 60], the radiation source behind the observation that diffuse Hα emission is ubiquitous throughout the Galaxy and widespread sources of flux shortward of 912 Å are required [59], and the source of ionization of the interstellar medium (ISM) wherein a large component of the baryonic matter of the universe is in the form of WHIM (warm-hot ionized media) in the absence of a conventional ionizing energy source [61, 62, 67]. Moreover, recent X-ray absorption data reveals that the temperature of galactic halo gas is in the range of 86 eV to 215 eV which is in the realm of the energy released for the transition of H to H(1/4) [67]. Indirect emission from ions of nonthermal origin is a feature of the continuum radiation emitted from hydrino transitions in celestial sources as well as hydrogen pinch plasmas at oxidized electrodes and solid fuel plasmas in our laboratory.

Rather than the mechanism of electric field acceleration of ions to cause dense emission of highly ionized ions as the source of the 10–30 nm continuum radiation of hydrogen plasmas, the ion line emission on top of the continuum was determined to be due to secondary emission of absorbed continuum radiation as in the case of astronomical sources. The emission in both cases was determined to be of non-thermal nature. Moreover, the 10–30 nm EUV continuum was observed in our laboratory from plasma having essentially no field. The HOH catalyst formed in the SF-CIHT cell was further shown to give 10.1 nm short-wavelength cutoff EUV continuum radiation of the same nature as in the pinch plasmas by igniting a solid fuel source of H and HOH catalyst by passing an ultra-low voltage, high current through the fuel to produce explosive plasma.

No chemical reaction can release such high-energy light, and the electric field corresponded to an applied voltage of less than 15 V for dense collisional plasma conditions immediately following the blast. A blast-induced electromagnetic pulse (EMP) of about the same voltage as measured on the ignition electrodes was observed with an independent electrode 2 m from the blast. EMPs were also observed on occasion with secondary blasts at times when the current was zero and no reactive voltage was possible. Furthermore, no reactive circuit voltage was created across the plasma as indicated by the exponential current decay with the measured L/R_0 time constant of the circuit in the pre-ignition state. The input energy during the blast E

given by

$$E = \int_0^\infty I^2 R \mathrm{d}t = R \int_0^\infty \left(I_0 \mathrm{e}^{-\frac{t}{\tau}} \right)^2 \mathrm{d}t = \frac{1}{2} R_0 I_0^2 \tau; \ \tau = \frac{L}{R_0} \tag{35}$$

was low, less than 20 J. The electric field was confined between the electrodes, and the plasma expanded at sound speed or greater. The plasma had to expand into vacuum away from the electrodes to be sufficiently optical thin to observe soft X-ray emission. Thus, essentially all of the emission occurred outside of the electrode region. The electron temperature was consequently low, about 1 eV, a factor of 100 times less than required to support the observed >100 eV continuum radiation. It is difficult to achieve this high an electron temperature even at low densities, and it is extremely improbable to be formed at solid to atmospheric high densities of the solid fuel plasmas by a conventional means. No high field existed to form highly ionized ions that could give radiation in this region. Moreover, as shown in Figure 8(B), following ignition, high-power plasma was observed with no power input. In cases, the amount of soft X-ray energy exceeded the total input energy to the plasma. The high ionization, the blackbody temperature of over 5000 K, and the massive high energy and visible light emission during phases of the ignition event requires an ionization source, a high energy source, and a high power source, all other than those provided by the electrical input. Controls showed no soft X-ray emission. This plasma source serves as strong evidence for the existence of the transition of H to hydrino H(1/4) by HOH as the catalyst as a new energy source. The H_2O-based solid fuels behave as energetic materials of extraordinarily high power density with most of the energy released as high energy light versus pressure-volume work. This aspect can be appreciated by comparison of high-speed video recordings of hydrino-based (Figure 8(A) and (B) and conventional explosives that show billowing smoke and fire [83, 84].

Based on a spectroscopically measured Stark line broadening, during a phase of the ignition event, the H_2O-based fuel ignition produces brilliant light-emitting plasma, an essentially fully ionized gaseous physical state of the fuel comprising essentially positive ions and free electrons. The blackbody temperature the ignition plasma was as high as that of the Sun, over 5000 K. Section 4.9 discusses the evidence that a portion of the Sun's power may be from hydrino reactions. The temperature of high explosives is also as high as 5500 K [38, 39]. This is expected if the source of the high temperature is the formation of hydrinos as supported by the observed massive soft X-ray emission and excessive EUV energy balance (section 4.6), excessive calorimetrically measured energy balance [7] having an ignition energy of about 5 J and a typical excess energy of about 200 J to 300 J per 40 mg solid fuel, and spectroscopic signatures of hydrinos [7, 8–14, 30–32]. Since solar cells have been optimized to convert blackbody radiation of 5800 K into electricity, photovoltaic conversion using solar cells is a

suitable means of power conversion of the SF-CIHT generator as confirmed by these tests. Simply replacing the consumed H_2O regenerated the fuel, and the fuel can be continuously fed into the electrodes to continuously output power.

The SF-CIHT cell power is in the form of light that may have a similar spectral composition as sunlight but at extraordinary power equivalent to 50,000 times the Sun's intensity at the Earth's surface. With the discovery of the photovoltaic effect by Becquerel in 1839 and the invention of the first modern solar cell by Chapin, Fuller, and Pearson of Bell Labs, an era of cheap clean energy from the Sun was envisioned for mankind. Realization of that vision is enabled by the invention of the SF-CIHT cell that overcomes the impediment of the very low power density of sunlight. With advances since its inception, solar cells have demonstrated the capacity to convert light into electricity at thousands of times higher power levels than sunlight intensity. Moreover, the cells operate at higher efficiency at the higher versus lower illumination intensities. At 50,000 times brighter than sunlight, the corresponding reduction in the area of the photovoltaic converter gives rise to a projected cost of the SF-CIHT generator of about $100/kW compared to over ten times that for conventional power sources of electricity. The safe, nonpolluting SF-CIHT cell uses cheap, abundant, nontoxic, commodity chemicals, with no apparent long-term supply issues that might preclude commercial, high volume manufacturing. Applications and markets for the SF-CIHT cell extend across the global power spectrum, including thermal, stationary electrical power, motive, and defense. Initial prototypes to generate extraordinary optical power by the formation of hydrinos are already producing photovoltaic generated electrical power.

References

[1] R. Mills *The Grand Unified Theory of Classical Physics* September 2016 Edition posted at http://brilliantlightpower.com/book-download-and-streaming/

[2] R. L. Mills, Y. Lu 2010 Int. J. Hydrogen Energy **35** 8446

[3] R. L. Mills, Y. Lu, K. Akhtar 2010 Cent. Eur. J. Phys. **8** 318

[4] R. L. Mills, Y. Lu 2011 Eur. Phys. J. D **64** 65

[5] R. L. Mills, R. Booker, Y. Lu 2013 J. Plasma Physics **79** 489

[6] A. Bykanov "Validation of the observation of soft X-ray continuum radiation from low energy pinch discharges in the presence of molecular hydrogen" http://www.blacklightpower.com/wp-content/uploads/pdf/GEN3_Harvard.pdf

[7] R. Mills J. Lotoski 2015 Int. J. Hydrogen Energy **40** 25

[8] K. Akhtar, J. Scharer, R. L. Mills 2009 Journal of Physics D: Applied Physics **42** 135207

[9] R. Mills, K. Akhtar 2009 Int. J. Hydrogen Energy **34** 6465

[10] R. L. Mills, B. Dhandapani, K. Akhtar 2008 Int. J. Hydrogen Energy **33** 802

[11] R. Mills, P. Ray, B. Dhandapani 2006 J. Plasma Physics **72** 469
[12] J. Phillips, C-K Chen, K. Akhtar, B. Dhandapani, R. Mills 2007 Int. J. Hydrogen Energy **32** 3010
[13] R. L. Mills, P. C. Ray, R. M. Mayo, M. Nansteel, B. Dhandapani, J. Phillips 2005 J. Plasma Physics **71** 877
[14] R. L. Mills, K. Akhtar 2010 Int. J. Hydrogen Energy **35** 2546
[15] M. Kuraica, N. Konjevic 1992 Physical Review A **46** 4429
[16] M. Kuraica, N. Konjevic, M. Platisa and D. Pantelic 1992 *Spectrochimica Acta* **47** 1173
[17] I. R. Videnovic, N. Konjevic, M. M. Kuraica 1996 Spectrochimica Acta Part B **51** 1707
[18] S. Alexiou, E. Leboucher-Dalimier 1999 Phys. Rev. E **60** 3436
[19] S. Djurovic, J. R. Roberts 1993 J. Appl. Phys. **74** 6558
[20] S. B. Radovanov, K. Dzierzega, J. R. Roberts, J. K. Olthoff 1995 Appl. Phys. Lett. **66** 2637
[21] S. B. Radovanov, J. K. Olthoff, R. J. Van Brunt, S. Djurovic 1995 J. Appl. Phys. **78** 746
[22] G. Baravian, Y. Chouan, A. Ricard, G. Sultan, 1987 J. Appl. Phys. **61** 5249
[23] A. V. Phelps, 1992 J. Phys. Chem. Ref. Data, **21** 883
[24] C. Barbeau, J. Jolly 1990 Journal of Physics D: Applied Physics, **23** 1168
[25] S. A. Bzenic, S. B. Radovanov, S. B. Vrhovac, Z. B. Velikic, and B. M. Jelenkovic 1991 Chem. Phys. Lett. **184** 108
[26] E. L. Ayers, W. Benesch 1988 Physical Review A **37** 194
[27] W. Benesch E. Li 1984 Optic Letters **9** 338
[28] R. Mills "Power generation systems and methods regarding same" PCT/IB2014/058177
[29] A. F. H. van Gessel Masters Thesis: *EUV spectroscopy of hydrogen plasmas* April 2009 Eindhoven University of Technology, Department of Applied Physics, Group of Elementary Processes in Gas Discharges EPG 09-02 p.61-70
[30] R. Mills, X Yu, Y. Lu, G Chu, J. He, J. Lotoski 2014 Int. J. Energy Res. **38** 1741
[31] R. Mills, J. Lotoski, W. Good, J. He 2014 Int. J. Hydrogen Energy **39** 11930
[32] R. Mills, J. Lotoski, J. Kong, G. Chu, J. He, J. Trevey 2014 Int. J. Hydrogen Energy **39** 14512
[33] T. J. Awe, B. S. Bauer, S. Fuelling, I. R. Lindemuth, R. E. Siemon 2010 Physics of Plasmas, **17** 102507
[34] J. Clementson "Interpretation of EBIT data-The case of tungsten," Lawrence Livermore National Laboratory presentation, slide 7
[35] E. Trabert 2002 Canadian Journal of Physics **80** 1481
[36] A. Phelps, J. Clemetson 2012 Eur. Phys. J. D **66** 120
[37] H-D Ngo "Pressure measurement in combustion engines" http://www-mat.ee.tu-berlin.de/research/sic_sens/sic_sen3.htm

[38] R. Simpson "Unraveling the mystery of detonation," https://www.llnl.gov/str/Simpson99.html

[39] R. Meyer, J. Kohler, A. Homburg "Explosives", Sixth Edition, 2007 Wiley-VCH Verlag GmbH & Co. KGaA, Weinheim p.119

[40] R.M. van der Horst, T. Verreycken, E.M. van Veldhuizen "P.J. Bruggeman, "Time-resolved optical emission spectroscopy of nanosecond pulsed discharges in atmospheric pressure N_2 and N_2/H_2O mixtures" arXiv:1403.5259v1 [physics.plasm-ph], 20 Mar 2014

[41] M. A. Gigosos, M. A. Gonzalez, V. Cardenoso 2003 Spectrochimica Acta Part B **58** 1489

[42] A. Fridman, L. A. Kennedy *Plasma Physics and Engineering* Second Edition, CRC Press, 2011 Taylor & Francis, NY, ISBN 9781439812280

[43] A. Beiser *Concepts of Modern Physics* Fourth Edition, 1978 McGraw-Hill Book Company New York p.329-340

[44] M. Masnavi, M. Nakajima, A. Sasaki, E. Hotta, K. Horioka 2005 Applied Physics Letters **87** 111502

[45] J. Pan, Y. Sun, P. Wan, Z. Wang, X. Liu 2005 Electrochemistry Communications **7** 857-862

[46] D. R. Lide *CRC Handbook of Chemistry and Physics* 88th Edition CRC Press, 2007 Taylor & Francis, Boca Raton, ISBN 0-8493-0488-1

[47] J. A. Dean *Lange's Handbook of Chemistry* Fifteenth Edition, 1999 McGraw-Hill Professional, New York

[48] O. Knacke, O. Kubascheeski, K. Hesselmann *Thermochemical Properties of Inorganic Substances* 2nd Ed., 1991 Springer-Verlag Berlin, Heidelberg

[49] G. F. Kinney, K. J. Graham *Explosive Shocks in Air*, Second Edition, 1985 Springer Science + Business Media, LLC

[50] M. A. Barstow and J. B. Holberg *Extreme Ultraviolet Astronomy* 2003 Cambridge Astrophysics Series 37, Cambridge University Press, Cambridge, Chapter 1, Figure 1.2.

[51] M. A. Barstow and J. B. Holberg *Extreme Ultraviolet Astronomy* 2003 Cambridge Astrophysics Series 37 Cambridge University Press Cambridge Chp.8

[52] R. Mills 2001 Int. J. Hydrogen Energy **26** 1041

[53] M. Stix, *The Sun* 1991 Springer-Verlag, Berlin, Figure 9.5, p.321

[54] Phillips, J. H. *Guide to the Sun* 1992 Cambridge University Press, Cambridge, Great Britain, p.126-127

[55] M. Stix *The Sun* 1991 Springer-Verlag, Berlin p.351-356

[56] http://nobelprize.org/nobel_prizes/physics/articles/bahcall/

[57] N. Craig, M. Abbott, D. Finley, H. Jessop, S. B. Howell, M. Mathioudakis, J. Sommers, J. V. Vallerga, R. F. Malina 1997 The Astrophysical Journal Supplement Series **113** 131

[58] E. M. Reeves, E. C. M. Huber, G. J. Timothy 1977 Applied Optics **16** 837

[59] S. Labov, S. Bowyer 1991 The Astrophysical Journal **371** 810

[60] S. Bower, G. Field, and J. Mack 1968 Nature **217** 32

[61] C. W. Danforth, J. M. Shull 2008 The Astrophysical Journal **679** 194

[62] N. Werner, A. Finoguenov, J. S. Kaastra, A. Simionescu, J. P. Dietrich, J Vink, H. Böhringer 2008 Astronomy & Astrophysics Letters **482** L29

[63] E. Bulbul, M. Markevitch, A. Foster, R. K. Smith M. Loewenstein, S. W. Randall 2014 The Astrophysical Journal **789** 13

[64] A. Boyarsky, O. Ruchayskiy, D. Iakubovskyi, J. Franse "An unidentified line in X-ray spectra of the Andromeda galaxy and Perseus galaxy cluster" 2014 arXiv:1402.4119 [astro-ph.CO]

[65] R. Stern, S. Bowyer 1979 Astrophys. J. **230** 755

[66] S. Bowyer, J. J. Drake, S. Vennes 2000 Ann. Rev. Astron. Astrophys. **38** 231

[67] A. Gupta, S. Mathur, Y. Krongold, F. Nicastro, M. Galeazzi 2012 The Astrophysical Journal Letters 756 L8

[68] F. Bournaud, P. A. Duc, E. Brinks, M. Boquien, P. Amram, U. Lisenfeld, B. Koribalski, F. Walter, V. Charmandaris 2007 Science **316** 1166

[69] B. G. Elmegreen 2007 Science **316** 32

[70] P. Jean, et al 2003 Astron, Astrophys. **407** L55

[71] M. Chown "Astronomers claim dark matter breakthrough" NewScientist.com, Oct. 3, 2003 http://www.newscientist.com/article/dn4214-astronomers-claim-dark-matter-breakthrough.html

[72] C. Boehm, D. Hooper, J. Silk, M. Casse, J. Paul 2004 Phys. Rev. Lett. **92** 101301

[73] G. H. Share 1991 Advances in Space Research **11** 85

[74] G. H. Share, R. L. Kinzer, D. C. Messina, W. R. Purcell, E. L. Chupp, D. J. Forrest, E. Rieger 1986 Advances in Space Research **6** 145

[75] B. Kozlovsky, R. E. Lingenfelter, R. Ramaty 1987 The Astrophysical Journal **316** 801

[76] E. P. Mazets, S. V. Golenetskii, V. N. Il'inskii, R. L. Aptekar', Y. A. Guryan 1979 Nature **282** 587

[77] G. H. Share, E. L. Chupp, D. J. Forrest, E. Rieger in *Positron and Electron Pairs in Astrophysics* ed. M. L. Burns, A. K. Harding, R. Ramaty "Positron annihilation radiation from Solar flares" 1983 New York: AIP, 15-20

[78] M. J. Jee, et al. 2007 Astrophysical Journal **661** 728

[79] R. L. Mills *The Grand Unified Theory of Classical Quantum Mechanics*, November 1995 Edition HydroCatalysis Power Corp. Malvern, PA Library of Congress Catalog Number 94-077780 Chp.22 ISBN number ISBN 0-9635171-1-2

[80] M. J. Jee, A. Mahdavi, H. Hoekstra, A. Babul, J. J. Dalcanton, P. Carroll, P. Capak 2012

Astrophys. J. **747** 96

[81] D. S. Akerib, et al "First results from the LUX dark matter experiment at the Stanford Underground Research Facility" 2014 http://arxiv.org/abs/1310.8214

[82] G. Agakishiev, A. Balanda, D. Belver, A. Belyaev, J.C. Berger-Chen, A. Blanco, M. Böhmer, J.L. Boyard, P. Cabanelas, S. Chernenko, A. Dybczak, E. Epple, L. Fabbietti, O. Fateev, P. Finocchiaro, P. Fonte, J. Friese, I. Fröhlich, T. Galatyuk, J.A. Garzón, R. Gernhäuser, K. Göbel, M. Golubeva, D. González-Díaz, F. Guber, M. Gumberidze, T. Heinz, T. Hennino, R. Holzmann, A. Ierusalimov, I. Iori, A. Ivashkin, M. Jurkovic, B. Kämpfer, T. Karavicheva, I. Koenig, W. Koenig, B.W. Kolb, G. Kornakov, R. Kotte, A. Krása, F. Krizek, R. Krücken, H. Kuc, W. Kühn, A. Kugler, A. Kurepin, V. Ladygin, R. Lalik, S. Lang, K. Lapidus, A. Lebedev, T. Liu, L. Lopes, M. Lorenz, L. Maier, A. Mangiarotti, J. Markert, V. Metag, B. Michalska, J. Michel, C. Müntz, L. Naumann, Y.C. Pachmayer, M. Palka, Y. Parpottas, V. Pechenov, O. Pechenova, V. Petousis, J. Pietraszko, W. Przygoda, B. Ramstein, A. Reshetin, A. Rustamov, A. Sadovsky, P. Salabura, T. Scheib, H. Schuldes, A. Schmah, E. Schwab, J. Siebenson, Yu.G. Sobolev, S. Spataro, B. Spruck, H. Ströbele, J. Stroth, C. Sturm, A. Tarantola, K. Teilab, P. Tlusty, M. Traxler, R. Trebacz, H. Tsertos, T. Vasiliev, V. Wagner, M. Weber, C. Wendisch, J. Wüstenfeld, S. Yurevich, Y. Zanevsky 2014 Physics Letters B **731** 365 DOI: 10.1016/j.physletb.2014.02.035

[83] http://www.youtube.com/watch?v=ni4qXAPtrlw

[84] https://www.youtube.com/watch?v=HFsAbkkAV-Q